ORNL
MASTER COPY

DATE ISSUED JAN 21 1974

ORNL-4926

AN ANALYSIS OF CHEMICAL FAILURE OF COATED UO_2 AND OTHER OXIDE FUELS IN THE HIGH-TEMPERATURE GAS-COOLED REACTOR

T. B. Lindemer
H. J. de Nordwall

OAK RIDGE NATIONAL LABORATORY
OPERATED BY UNION CARBIDE CORPORATION • FOR THE U.S. ATOMIC ENERGY COMMISSION

Printed in the United States of America. Available from
National Technical Information Service
U.S. Department of Commerce
5285 Port Royal Road, Springfield, Virginia 22151
Price: Printed Copy $5.45; Microfiche $1.45

This report was prepared as an account of work sponsored by the United States Government. Neither the United States nor the United States Atomic Energy Commission, nor any of their employees, nor any of their contractors, subcontractors, or their employees, makes any warranty, express or implied, or assumes any legal liability or responsibility for the accuracy, completeness or usefulness of any information, apparatus, product or process disclosed, or represents that its use would not infringe privately owned rights.

ORNL-4926
UC-77 Gas Cooled Reactor Technology

Contract No. W-7405-eng-26

CHEMICAL TECHNOLOGY DIVISION

Chemical Development Section A

AN ANALYSIS OF CHEMICAL FAILURE OF COATED UO_2 AND OTHER OXIDE FUELS IN THE HIGH-TEMPERATURE GAS-COOLED REACTOR

T. B. Lindemer

H. J. de Nordwall

JANUARY 1974

OAK RIDGE NATIONAL LABORATORY
Oak Ridge, Tennessee 37830
operated by
UNION CARBIDE CORPORATION
for the
U.S. ATOMIC ENERGY COMMISSION

CONTENTS

Page

ABSTRACT 1

1. INTRODUCTION 1

2. THERMODYNAMIC BEHAVIOR OF UNIRRADIATED OXIDE FUEL SYSTEMS. . . . 3

2.1 Thermodynamics of the $C-CO-CO_2-O_2$ System. 3

2.2 Thermodynamics of the Oxide Fuels 5

2.2.1 $UO_{2\pm x}$. 5

2.2.2 $(U,Pu)O_{2\pm x}$ 7

2.2.3 ThO_2 9

2.2.4 $(U,Th)O_{2+x}$ 11

3. CHEMISTRY OF THE IRRADIATED FUEL OXIDE—FISSION PRODUCT SYSTEM. . 11

3.1 Calculation of Oxygen Release in Oxide Fuels. 12

3.2 Measurement of Oxygen Release in Oxide Fuels. 14

3.3 Additional Chemical Equilibria in Oxide Particles 18

4. MASS TRANSPORT IN OXIDE PARTICLES IN A TEMPERATURE GRADIENT. . . 21

4.1 The Dragon Project Empirical Correlation. 21

4.2 First-Principle Derivations of Oxide Particle Transport Models. 25

4.2.1 Calculated Rate of Carbon Transport by $CO-CO_2$ Diffusion 26

4.2.2 Calculated Rate of Carbon Transport Controlled by Carbon Monoxide Disproportionation 33

4.2.3 Rate of Carbon Deposition or Kernel Migration by Solid-State Diffusion Mechanisms. 38

4.3 Theoretical Basis for Correlation of Irradiation Data . . . 39

4.4 Methods for Determination of the Rate-Controlling Mechanism 42

4.5 Analysis of Experimental Data 48

CONTENTS (continued)

Page

5. SUMMARY OF OXIDE FUEL BEHAVIOR 54

6. ACKNOWLEDGMENTS. 56

7. APPENDIX A: THERMODYNAMIC DATA FOR FUEL OXIDES AND CARBIDES. 57

8. APPENDIX B: DERIVATION OF EQUATIONS FOR TRANSPORT OF CARBON BY $CO-CO_2$ DIFFUSION. 59

9. DEFINITION OF SYMBOLS. 71

10. REFERENCES 75

AN ANALYSIS OF CHEMICAL FAILURE OF COATED UO_2 AND OTHER OXIDE FUELS IN THE HIGH-TEMPERATURE GAS-COOLED REACTOR

T. B. Lindemer and H. J. de Nordwall

ABSTRACT

The thermodynamic data for unirradiated dioxides in the U-Th-Pu-O system are briefly reviewed. Calculations of oxygen release during fission were made and were found to agree qualitatively with experimental measurements. Theories were developed for prediction of mass transport rates in oxide particles; these included control by either CO-CO_2 diffusion, reactions such as disproportionation of carbon monoxide, or solid-state diffusion through the kernel. Methods were devised for the determination of the general type of rate-controlling mechanism from the quantitative analysis of in-reactor and out-of-reactor experiments. Application of these methods to an in-pile experiment indicated that CO-CO_2 diffusion did not control the rate of UO_2 or $(Th,U)O_2$ migration in BISO particles; instead, control by solid-state diffusion was indicated.

---

1. INTRODUCTION

Fuel elements for high-temperature gas-cooled reactors (HTGRs) are made from rigid assemblies (fuel sticks or compacts) of coated fuel particles distributed appropriately in graphite holders that contain coolant passages and constitute both moderator and core structure.[1-3] The coated fuel particles consist of small spherical oxide or carbide kernels that are each coated with successive layers of pyrolytic carbon ("BISO" particles) and sometimes an intermediate layer of silicon carbide ("TRISO" particles). The pyrolytic carbon layers absorb damaging fission fragments and retain gaseous fission products and their precursors, while the

silicon carbide layer improves the retention of metallic fission products and fuels.[4,5] These fuels are currently designed to operate from 700°C to a nominal maximum of 1550°C, the latter temperature being sustained for times that are much smaller than the core lifetime. When a sufficient temperature gradient is imposed across the particle at an appropriately high temperature, the coatings are observed to fail with the subsequent deleterious release of fission products. This failure is sometimes observed to be associated with a lateral migration of the fuel kernel into the coatings, the so-called "amoeba effect."

Numerous models describe the mechanical behavior of these systems under isothermal conditions[6-8] and have been used as aids in the design of coated particles since 1964. Detailed testing of these models is restricted by a shortage of well-defined data relating to primary parameters and their variation with temperature and manufacturing variables. Moreover, each of the models arbitrarily excludes chemical effects.

In this report models are developed for the chemical design of oxide particles. These models correlate the experimental information available for the failure of the coating via the "amoeba effect" under reactor conditions, the effects of fission gas and "oxygen" release during nuclear fission, and measurements of carbon monoxide pressures in irradiated uranium dioxide particles; the resulting analyses are an extension of an earlier analysis by Flowers and Horsley.[9] Specifically, Sections 2 and 3 consider thermodynamic factors that may influence fuel and coating stability. In Section 4 the discussion of particle integrity is widened to consider potential kinetic limitations and possible methods of ascertaining the rate-controlling mechanisms for fuel and carbon transport. In Section 5

these methods are applied to the quantitative measurement of fuel oxide migration observed in particles irradiated in fuel rods and tentative conclusions are drawn concerning the rate-controlling mechanism for this migration.

2. THERMODYNAMIC BEHAVIOR OF UNIRRADIATED OXIDE FUEL SYSTEMS

The unirradiated fuel particle consists of an oxide fuel kernel, a porous layer of carbon, and layers of dense pyrocarbon and sometimes SiC. One may reasonably assume that the fuel within the coated particle reaches thermodynamic equilibrium with the surrounding coatings at the service temperature; this is most readily envisioned as the $C-CO-CO_2-MO_{2\pm x}$ equilibrium, where M is U, Th, Pu, or their usual combinations, and fission products. The complexities of the system can be best understood by considering separately the variation in chemical potential* of oxygen, $\mu_O = RT \ln P_{O_2}$, of the components under the conditions that may exist within the particle.

2.1 Thermodynamics of the $C-CO-CO_2-O_2$ System

The oxygen potential at specific conditions in the $C-CO-CO_2-O_2$ system will be considered first because overpressures of the gases exist in oxide fuel particles. As will be shown later, these overpressures lead to control of oxygen-to-metal ratios in the oxide fuels. The value of the oxygen potential in the $C-CO-CO_2-O_2$ system as a function of specific $P_{CO} + P_{CO_2}$ values and temperature has been calculated from data in the JANAF Tables[10] and is shown in Fig. 1 (solid lines). The oxygen potential at specific

---

*Subsequently, "oxygen potential" will be used to signify "chemical potential of oxygen."

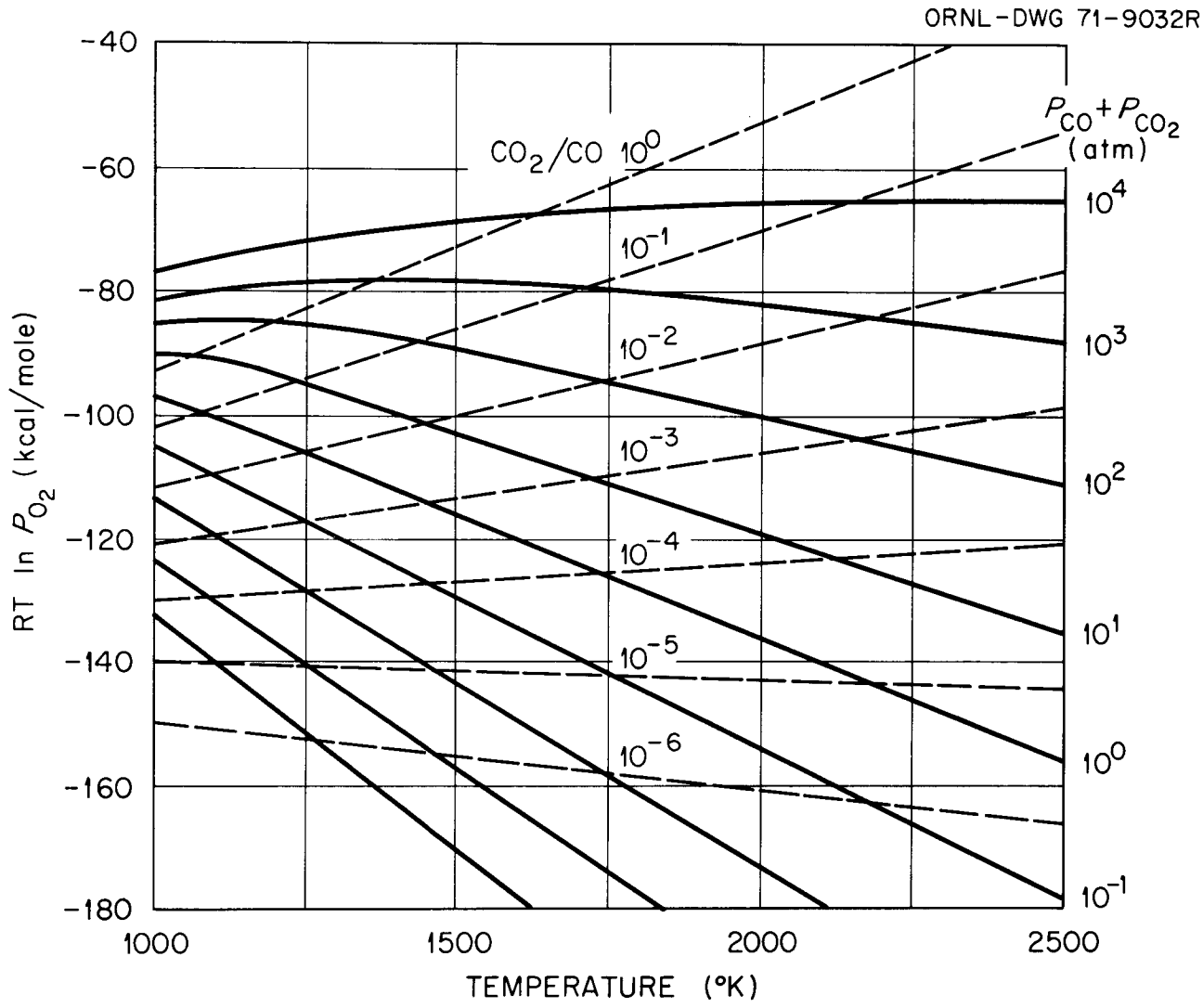

Fig. 1. The Temperature Dependence of the Oxygen Potential (RT ln P_{O_2}) for the C-CO-CO_2 Equilibrium at the Indicated Total Pressures of Carbon Monoxide and Carbon Dioxide or at the Indicated CO_2/CO Ratios.

values of P_{CO_2}/P_{CO} as a function of temperature is also given in Fig. 1 (dashed lines). It should be mentioned that the quantities shown in Fig. 1 are dependent only on the properties of the $C-CO-CO_2-O_2$ systems and are not dependent per se on the thermodynamic properties of an oxide fuel.

2.2 Thermodynamics of the Oxide Fuels

2.2.1 $UO_{2\pm x}$

The oxygen potentials for $UO_{2\pm x}$ have been reported by several different investigators.[11-15] The results of these studies are given in Fig. 2. The agreement for hyperstoichiometric oxide is quite good, while the agreement for an O/U of 1.99 is reasonable. The oxygen potential for stoichiometric UO_2 is shown as reported primarily by Rand and Markin[15] and Pattoret et al.;[13] because of the rapid change in oxygen potential as the O/U crosses a value of 2, the actual oxygen potential of stoichiometric UO_2 is difficult to define. For the present purposes, the exact definition is not critical. Below an O/M of 2.00, the agreement is not good and only the data of Pattoret et al.[13] have been plotted. The oxygen potential for the $UO_2-UC_{1.86}-C-CO$ equilibrium is also plotted in Fig. 2 because this equilibrium establishes the minimum oxygen potential possible in a carbon-coated particle containing UO_2 or UO_{2-x}.

Equilibration of UO_{2+x} with overpressures of carbon monoxide (P_{CO}) and carbon dioxide (P_{CO_2}) in a coated particle can be shown to limit the maximum value of x. The coated particle can be expected to fail from stresses generated at $P_{CO} + P_{CO_2}$ of the order of 1000 atm. From Fig. 1 this is seen to be equivalent to an oxygen potential of approximately -80 kcal/mole.

ORNL-DWG 71-9033R

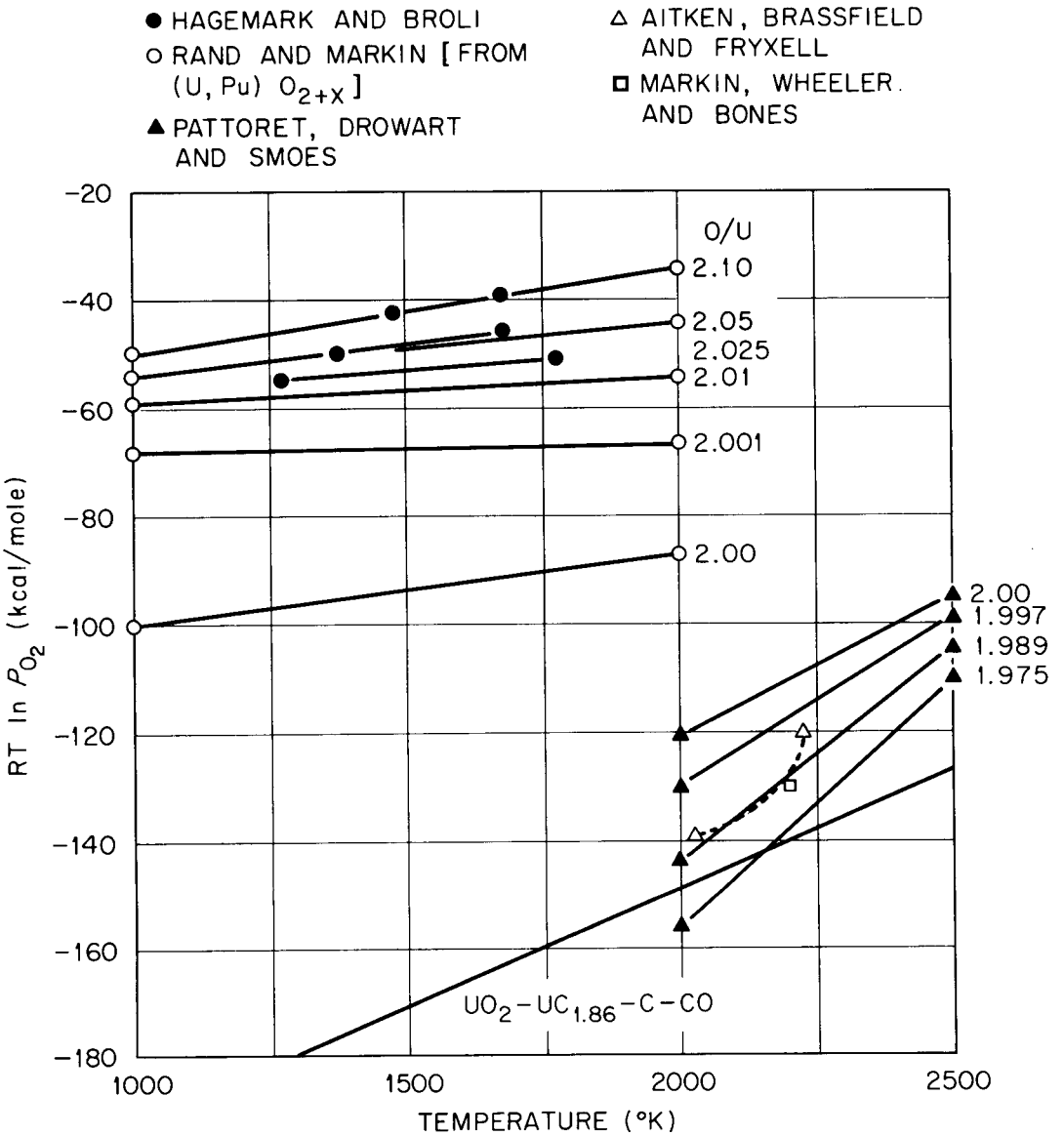

Fig. 2. The Temperature Dependence of the Oxygen Potential (RT ln P_{O_2}) for $UO_{2\pm x}$ at the Indicated O/U Ratios and for the UO_2-$UC_{1.86}$-C Equilibrium.

This is also the oxygen potential in equilibrium with a coated oxide kernel at a specific O/U ratio (Fig. 2). It can be seen that this O/U ratio is less than 2.001 in a coated particle. Thus, the stoichiometry change in UO_2 is not an effective "sink" for oxygen released during fission, a subject to be discussed in Sect. 3.1.

2.2.2 $(U,Pu)O_{2\pm x}$

Two primary investigations of the $(U,Pu)O_{2\pm x}$ system have been made. Markin and McIver[16] studied the system $(U,Pu)O_{2\pm x}$ at Pu/(Pu + U) values of 0.10 and 0.30 from 750°C to 1140°C and Woodley[17] investigated the system $(U,Pu)O_{2-x}$ at a Pu/(U + Pu) value of 0.25 from 950°C to 1400°C. Rand and Markin[15] made a further analysis of the data of Markin and McIver[16] and found an empirical relation between the average valence of plutonium (V_{Pu}), uranium (V_U), and the oxygen-to-metal ratio (O/M); this relation is

$$O/M = \frac{Y}{2} V_{Pu} + \frac{(1 - Y)}{2} V_U \quad , \qquad (1)$$

in which

$$Y = Pu/(U + Pu)$$

$$V_U = 4 \text{ for } O/M < 2$$

$$V_{Pu} = 4 \text{ for } O/M > 2.$$

The oxygen potential as a function of V_{Pu} from these two investigations is shown in Fig. 3. It is clear that some discrepancy exists in the two sets of measurements, but this has not been resolved in the literature at the present time.

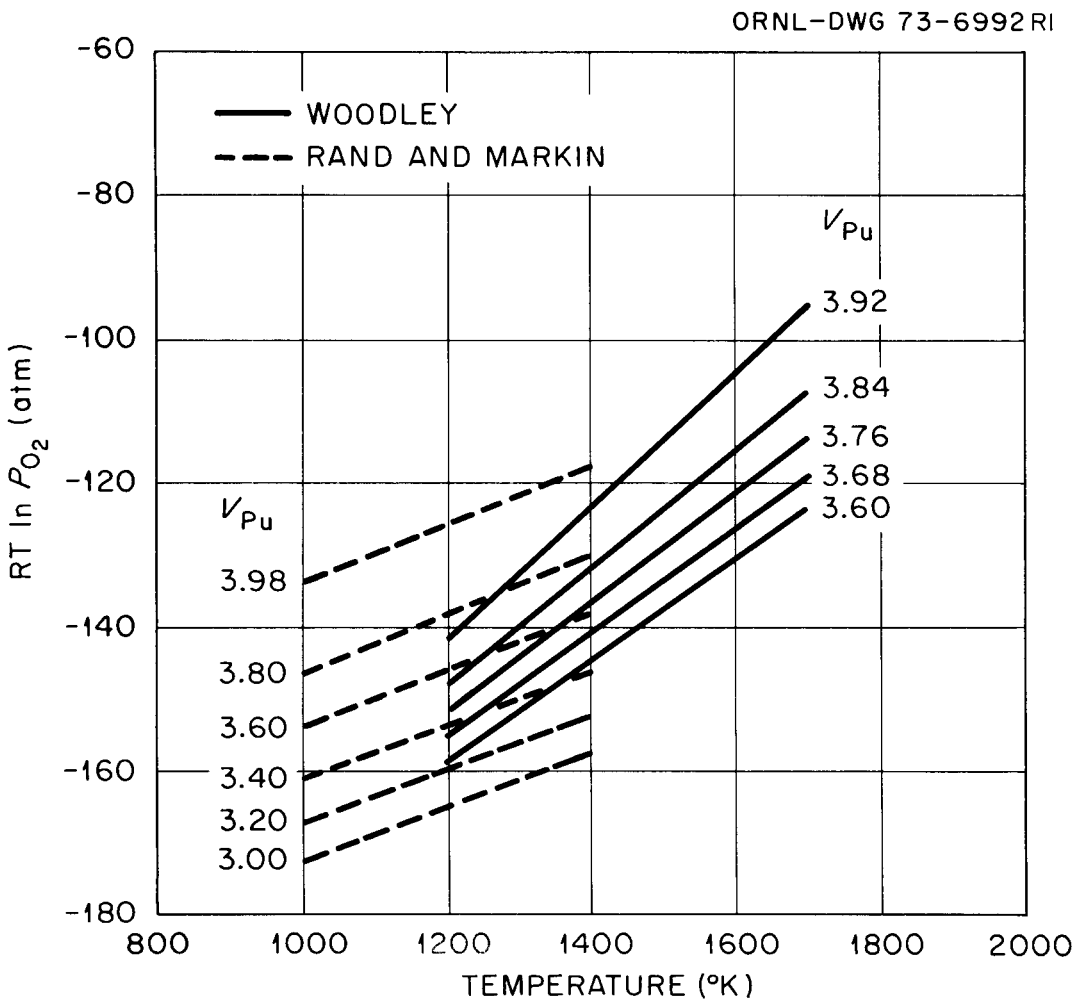

Fig. 3. Temperature Dependence of the Oxygen Potential (RT ln P_{O_2}) for $(U,Pu)O_{2-x}$ at the Indicated Valences of Plutonium.

The results of the analysis of the data for $(U,Pu)O_{2+x}$, using Eq. (1) by Rand and Markin,[15] are shown in Fig. 2; it can be seen that O/U in the mixed hyperstoichiometric oxide is essentially the same as that in pure UO_{2+x}.

A third investigation of the $(U,Pu)O_{2-x}$ system from 1000 to 1700°C has been reported by Javed and Roberts,[18] but their oxygen potentials at a given V_{Pu} are much lower than those in Fig. 3 and were thus not included. An analysis of the process for hydrogen reduction of $(U,Pu)O_2$ to $(U,Pu)O_{2-x}$ from 1400 to 1740°C has been performed by Lindemer and Bradley,[19] who used the oxygen potentials as extrapolated above 1100°C by Rand and Markin.[15] They found that the extrapolated oxygen potentials appeared to be too negative at a given V_{Pu}, which is in qualitative agreement with the measurements of Woodley[17] and which also appears to cast considerable doubt upon the measurements of Javed and Roberts.[18]

2.2.3 ThO_2

Thermodynamic data for the thoria system are sketchy. The ThO_2 phase does begin to exhibit slight hypostoichiometry at ~ 1700°C.[20] Ackermann *et al.*[21] have studied the evaporation behavior of the Th-O system from 2000 to 3000°K, and their calculation of the pressure of atomic oxygen over evaporating ThO_2 can be used to calculate the oxygen potential over ThO_2. The results of these calculations, along with the oxygen potential for the ThO_2-ThC_2-C-CO equilibrium, are shown in Fig. 4. Peterson and Curtis[22] have published an extensive compilation of the known properties of ThO_2 and other thorium compounds.

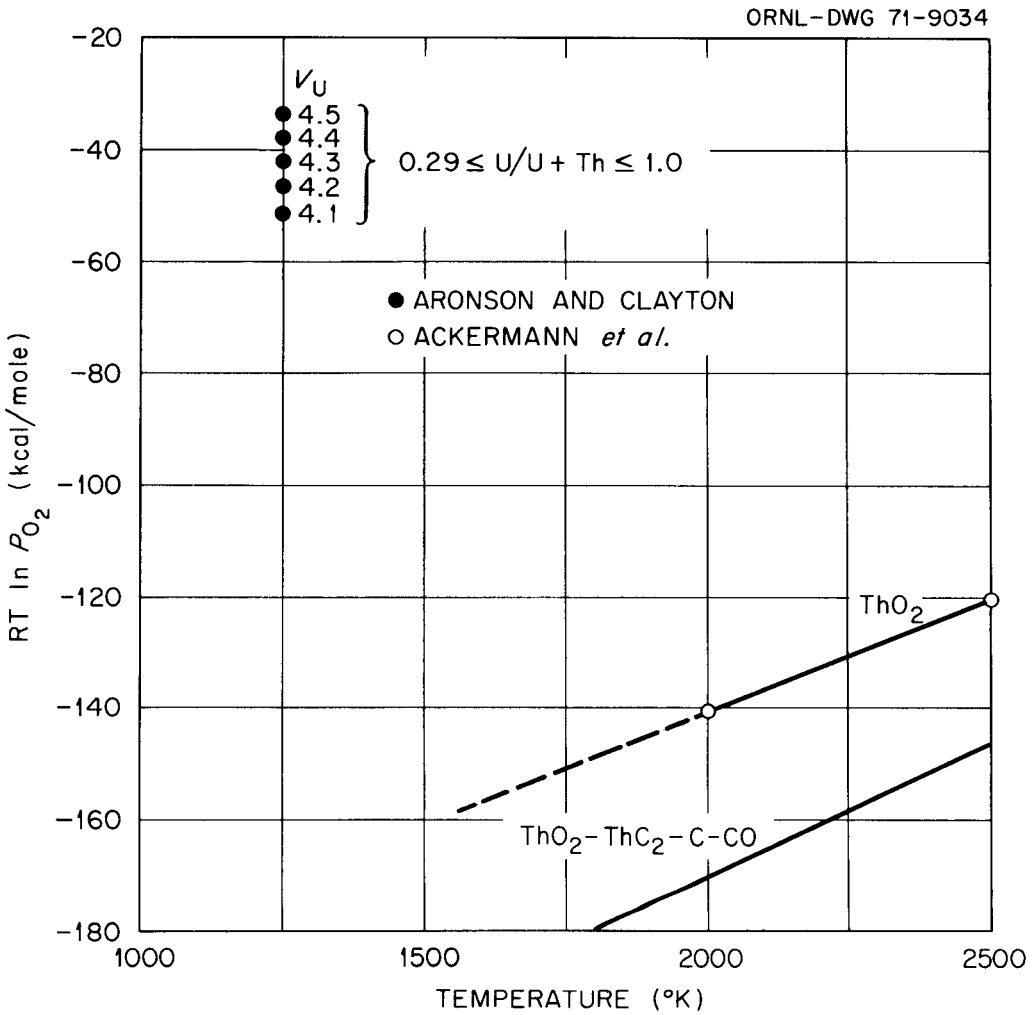

Fig. 4. Temperature Dependence of the Oxygen Potential (RT ln P_{O_2}) for the Thoria and Thoria-Urania Systems at the Indicated Compositions and for the ThO_2-ThC_2-C Equilibrium.

2.2.4 $(U,Th)O_{2+x}$

Aronson and Clayton[23] have investigated the thermodynamics of $(U,Th)O_{2+x}$ at 1250°K for U/(U + Th) ratios of 1, 0.9, 0.71, 0.52, and 0.29 and values of x from 0.02 to 0.16. The use of Eq. (1), with $V_{Th} = 4$ substituted for V_{Pu}, was assumed to be applicable to the UO_2-ThO_2 system and permits the calculation of V_U shown in the upper left portion of Fig. 4. Comparison at a given oxygen potential of V_U in Fig. 4 with $V_U = 2(O/U)$ in Fig. 2 indicates that the valence of uranium in the Th-U-O system is essentially the same as that shown in Fig. 2 for the U-O and U-Pu-O systems.

Thermodynamic functions for UO_2, ThO_2, and PuO_2, as well as for $UC_{1.93}$ and ThC_2, are given in Appendix A.

A comprehensive review of specific composition-dependent properties of oxides has been published by Kofstad.[24] This work includes the fuel oxides and rare-earth oxides.

A parameter that may be important to the understanding of oxide fuel migration is the solubility of carbon in the oxides. This parameter has a value of the order of 100 ppm by weight, but the solubility as a function of temperature and O/M is not known.

3. CHEMISTRY OF THE IRRADIATED FUEL OXIDE—FISSION PRODUCT SYSTEM

The chemistry of the fuel oxide—fission product system is so complicated that very little definitive information on the specific thermodynamic behavior of the irradiated fuel system is available. On the other hand, one can calculate the approximate bounds of certain types of chemical behavior from the known properties of the elements that appear as fission

products. As will be shown later, the bounds on the value of P_{CO} as a function of burnup are two such calculable quantities, and these values can be more exactly defined by measurements of P_{CO} in irradiated particles. Since some of the failure mechanisms postulated to control the failure of oxide particles will be shown to be dependent upon P_{CO}, such predictions and measurements of P_{CO} have direct potential value in attempts to quantify the failure characteristics of oxide particles.

3.1 Calculation of Oxygen Release in Oxide Fuels

The amount of oxygen that is released to form carbon monoxide in a coated particle is the difference between the combined oxygen originally present in the spent fuel and the combined oxygen in the fission products. One may use tables of fission yields to determine the amount of each fission-product element present or may more accurately determine these amounts by using computer codes that consider such factors as contributions from medium-lived isotopes, capture effects, and mixtures of fertile and fissile isotopes in the initial fuel. As an example, the yields of heavy metals and fission product elements as a function of burnup were calculated with the ORIGEN Code[25] for ^{232}Th, 93%-enriched U, and PuO_2. The yields of fission products are used to calculate the oxygen present as metal monoxides (MO), sesquioxides ($MO_{1.5}$), and dioxides (MO_2). The primary uncertainty in the calculation of the number of bound oxygen atoms is the effective oxidation state of yttrium, lanthanum, and the lanthanides; these elements may form either $MO_{1.5}$ or MO_2 when in solid solution in UO_2. The results of the calculations are given in Table 1. Flowers and Horsley[9] have made similar estimates of the oxygen release from data

Table 1. Calculated Release of Oxygen, Krypton, and Xenon During Nuclear Fission of Oxide Fuel

(Yield given in atoms per thousand initial heavy metal atoms, except where noted)

Fuel	Flux (neutrons cm^{-1} sec^{-1})	Fission Gases			Heavy Metals						MO	MO_2	$MO_{1.5}$ or MO_2	Oxygen		
		Kr	Xe	Kr + Xe (atoms/fission)	U	Np	Pu	Th	Pa	Am	Sr + Ba	Zr + Ce + Nb	Y + La + Lanthanides	Bound in Fission Products	(atoms/fission) ORIGEN Calc.	(atoms/fission) Ref. 9
93%-Enriched UO_2	1.03×10^{14}															
Burnup, % FIMA:																
37.6		14.6	105	0.318	616	4.4	3.5				62.4	197.24	145.21	675-747	0.125-0.206	0.13-0.314[a]
73.7		27.9	203	0.314	221	21	21.5				117.0	345.39	300.9	1259-1409	0.088-0.292	
93%-Enriched UO_2	3.47×10^{13}															
Burnup, % FIMA:																
37.9		14.6	99.8	0.302	613	4.5	3.5				59.3	186.6	154.39	664-741	0.044-0.248	
73.8		27.4	194.0	0.300	219	20.9	21.8				124.4	342.13	312.45	1277-1433	0.058-0.269	
$^{232}ThO_2$	1.0×10^{14}															
Burnup, % FIMA:																
2.96		2.04	7.56	0.325	27.4			940	3.04		5.67	14.52	11.05	51.3-56.8	0.078-0.265	0.0813-0.264[b]
7.85		5.40	20.50	0.330	34.6			884	2.87		14.97	37.71	30.74	136.5-151.9	0.066-0.262	
$(^{239}PuO_{0.9}\,^{240}PuO_{0.1})O_2$	3.0×10^{13}															
Burnup, % FIMA:																
28.9		4	77	0.284			710			0.80	29.9	100.3	91.7	368.0-413.9	0.0568-0.726	0.624-0.786[b]
68.4		8.7	147	0.228			302			14.2	52.5	167.9	190.9	674.7-770.1	0.874-1.01	

[a]For HTGR flux, no burnup dependence specified; 25% Pu, 75% U initially.

[b]For HTGR flux, no burnup dependence specified.

obtained from fission-yield tables; their estimates are also given in Table 1 for the purpose of comparison.

Several general observations can be made about the oxygen release. It is immediately evident that fissioning of PuO_2 releases much more oxygen than does fissioning of ^{235}U or of ^{233}U derived from ^{232}Th. (In practice, PuO_{2-x} would be used as a fuel to partially offset this high release value.) It can also be discerned that more oxygen is released per fission at the later stages of burnup of uranium; again, this is probably caused by the breeding and subsequent fissioning of small amounts of plutonium (see Table 1) from ^{238}U. This latter effect can also be seen in the calculations of Flowers and Horsley[9] for the U-Pu mixture; their calculated oxygen release is higher than that calculated here for fully enriched UO_2.

3.2 Measurement of Oxygen Release in Oxide Fuels

Oxygen released during fissioning of oxide fuels reacts with carbon from the coating to form carbon monoxide. Since the coating layers in the particle act as a pressure vessel, the carbon monoxide is retained. A few measurements of the amounts of carbon monoxide present in irradiated particles have been made subsequent to irradiation by crushing individual particles at elevated temperatures in a mass spectrometer. Since the number of moles of carbon monoxide can be calculated from the measurements and the burnup is also known, one can use these data to calculate the oxygen release per fission.

Graham[26] has reported data for the volume of carbon monoxide released from Dragon Project reference UO_2 particles* irradiated to 6% FIMA (Fissions

*The particle coatings consist of an inner layer of low-density pyrocarbon, a layer of dense pyrocarbon, SiC, and an outer layer of dense pyrocarbon.

per Initial Heavy Metal Atom). This work was done by Bildstein and Strigl at SGAE Seibersdorf, where measurements were also made on unirradiated particles.[27] Their results have been used to calculate the oxygen release per fission shown in Table 2 for 9.7%-enriched UO_2 (Specimen CD 1032). It should be mentioned that several other sets of specimens that experienced up to 5% FIMA did not contain carbon monoxide pressures above those in the original, as-coated particles.[27]

Table 2. Experimental Oxygen Release, in Atoms per Fission

Temperature (°C)	Fuel Composition	
	9.7%-enriched UO_2 (6% FIMA)[a]	$Th_{0.75}U_{0.25}O_2$ (13% FIMA)[b]
920		0.017
1000	0.028	
1030		0.124
1100		0.065
1200		0.120
1300		0.230
1400	0.068	
1600	0.194	
1800	0.300	

[a]Ref. 27; Dragon Project reference particles.
[b]Ref. 28; TRISO I particles.

More recently, workers at Gulf General Atomic Division (GGA), Gulf Energy and Environmental Systems, Inc., have also made measurements of gas released from SiC-coated (TRISO I*) particles containing $Th_{0.75}U_{0.25}O_2$

*TRISO I particle coatings consist of a lower-density carbon buffer layer, SiC, and a dense pyrocarbon layer.[28]

irradiated to 13% FIMA.[28] In these experiments the total gas volume was measured and the volume of xenon and krypton was calculated from the fission product yields by assuming complete gas release. The difference between the total and the (Xe + Kr) volume was assumed to be carbon monoxide. Their results at specific temperatures were used here to calculate the average oxygen release per fission for $(U,Th)O_2$, as shown in Table 2.

The experimental oxygen release in Table 2 can be compared with the calculated results in Table 1. The experimental release usually appears to lie above the minimum calculated release, which indicates that a portion of the rare earth oxides exist as sesquioxides. As temperature is increased, the oxygen release appears to increase, which indicates that the amount of sesquioxide also increases. Because the resulting carbon monoxide pressure appears to range between 0.1 and 1.0 of the pressure of xenon and krypton, the pressure of carbon monoxide may be as important in the models for mechanical design of particles as it is in some of the proposed models for chemical design.

Bildstein and Strigl's[27] measurements also permit the calculation of the oxygen potential of both the as-coated and the irradiated particles. Their results have been converted to oxygen potentials at temperature by assuming equilibrium in the $C-CO-CO_2$ system and that the measured volume of carbon monoxide could be used to calculate P_{CO}; the void volume for gas containment in the oxide and the buffer layer was equal to 25% of the geometrical volume of the kernel.[27] The calculated oxygen potentials are shown in Fig. 5. It can be seen from Fig. 5 that the oxygen potential of the unirradiated and irradiated UO_2 particles ranged between

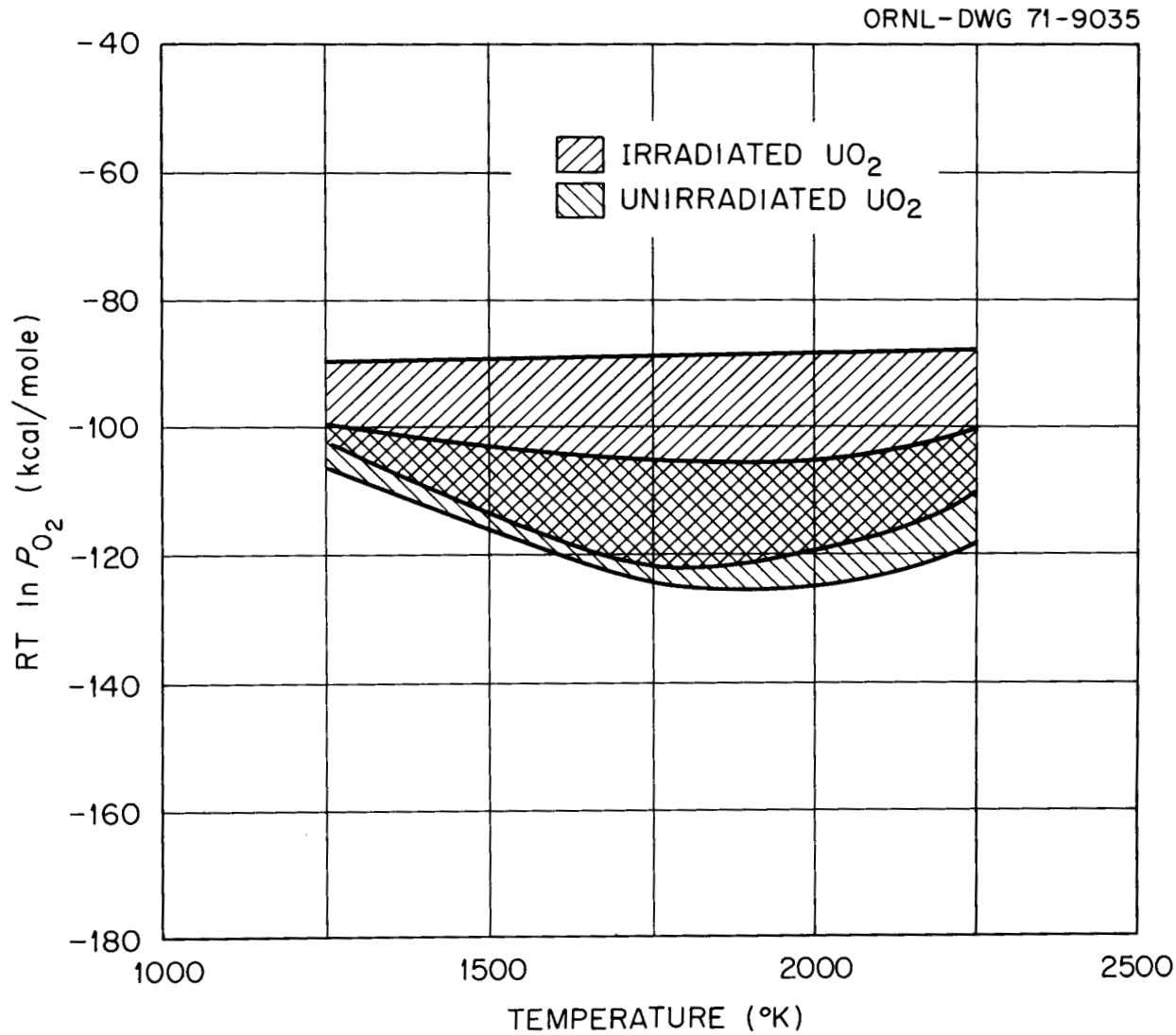

Fig. 5. The Oxygen Potentials (RT ln P_{O_2}) Calculated from Bildstein and Strigl's[27] Measurements of Carbon Monoxide Released from UO_2 Coated Particles Having a Void Volume Equal to 25% of the Kernel Volume.

-90 and -125 kcal/mole; from Fig. 2 this range indicates an O/U from an upper limit of 2.000 to < 2.001 for temperatures up to 2000°K to a lower limit of ~1.99 at higher temperatures. Although the oxide stoichiometry does not vary much in this range of oxygen potentials, an examination of Fig. 1 illustrates that the range of $P_{CO} + P_{CO_2}$ varies widely, from 1 to 30 atm at 1250°K and from 30 to 800 atm at 2250°K. In the unirradiated particles these pressures must originate from the reduction of slightly hyperstoichiometric UO_2 (O/U ~2.0015 for a = 0.25). Thus it is clear that reduction of the O/U ratio to exact stoichiometry in the initial kernel is important if the as-coated value of P_{CO} is to be minimized.

3.3 Additional Chemical Equilibria in Oxide Particles

Other chemical systems that could possibly affect the oxygen potential, and hence P_{CO}, are also present in coated particles. Silicon carbide, which is present as a coating layer in some fuel particles, would be exposed to carbon monoxide upon failure of the dense pyrocarbon layer that separates the kernel from the silicon carbide. Consequently, silicon carbide could react with carbon monoxide to establish the equilibrium

$$SiC + 2CO \rightleftarrows SiO_2 + 3C \quad .$$

The value of P_{CO} for this reaction (from data in the JANAF Tables[10]) is shown in Fig. 6. If the rate of the forward reaction were sufficiently rapid to permit equilibrium to be attained, then application of the phase rule demonstrates that P_{CO} would be controlled at a fixed value at a given temperature. Such a process is called chemical buffering; Flowers and Horsley[9] proposed silicon carbide additions to UO_2 kernels for exactly

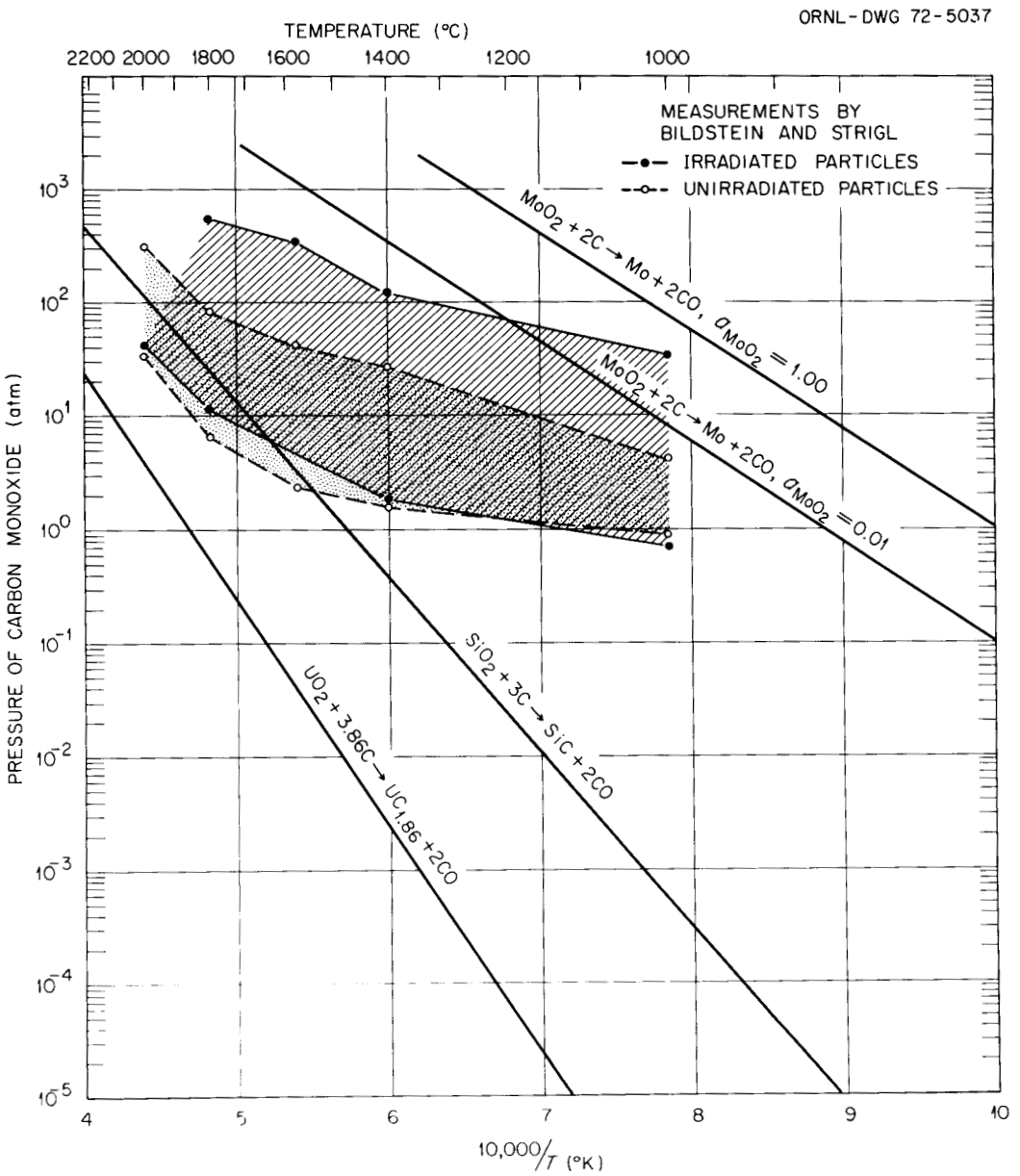

Fig. 6. Temperature Dependence of Carbon Monoxide Pressure for Indicated Equilibria. Also shown are the pressures calculated by Bildstein and Strigl[27] for Dragon Project reference particles having a void volume equal to 25% of the kernel volume.

this purpose. However, it can be seen from Fig. 6 that the P_{CO} measured by Bildstein and Strigl[27] in irradiated SiC-containing Dragon Project particles is generally much higher than that for the SiC-CO-SiO_2-C equilibrium. Consequently, either the forward reaction to form silica is too slow to attain equilibrium or the inner pyrocarbon layer remained intact. The measurements of P_{CO} at GGA in irradiated TRISO I particles, where the inner dense pyrocarbon layer is absent,[28] would indicate that the forward reaction is actually too slow to permit equilibrium. These several observations also indicate that an earlier analysis[29,30] which indicated control of the rate of failure of the Dragon Project particles by CO-CO_2 diffusion at the P_{CO} for this equilibrium was erroneous.

A second chemical system that could be proposed to chemically buffer P_{CO} involves fission-product molybdenum. The value of P_{CO} for the Mo-MoO_2-CO-C equilibrium is shown in Fig. 6 for two different activities of MoO_2, the lower activity being chosen to illustrate the effect of solution of molybdenum oxide in uranium dioxide. It can be seen that P_{CO} for this equilibrium at normal operating temperatures is probably greater than 100 atm. Thus this equilibrium is not capable of controlling P_{CO} at a low value, as is substantiated by the measurements of Bildstein and Strigl.[27]

There is general agreement in the literature that no other equilibria involving fission products have values of P_{CO} that lie between those for the two equilibria discussed above. Hence, in the absence of reaction with silicon carbide, an ever-increasing pressure of carbon monoxide is generated in a coated particle as the result of oxygen release during fission of oxide fuel. This may be an important effect both for the

hydraulic design of particles and for certain proposed carbon-transporting mechanisms in oxide coated particles.

4. MASS TRANSPORT IN OXIDE PARTICLES IN A TEMPERATURE GRADIENT

Numerous observations have been made of oxide kernel migration up the temperature gradient in irradiated particles and/or carbon deposition in the colder regions of these particles. A typical observation is shown in Fig. 7. Many attempts have been made to explain these observations by quantitative, first-principle models; several of these models will be discussed below. However, to date none of the attempts has been definitive, in contrast with the quantitative model developed for ThC_2 and UC_2 fuel particles.[31-33] Consequently, this section will present the state-of-the-art.

In this section a summary is made of the Dragon Project correlation for oxide particle failure and then several mathematical expressions are derived to quantitatively describe mass transport rates controlled by typical CO-CO_2 diffusion, gas-solid reaction, or solid-state diffusion mechanisms. These expressions are applied to the analysis of specific in-reactor and out-of-reactor experiments to ascertain which specific mechanism is controlling the rate of the observed mass transport.

4.1 The Dragon Project Empirical Correlation

The Dragon Project has produced a correlation for the failure of UO_2 particles under reactor conditions for the Dragon Reference Particle (800-μm kernel, 155-μm total coating thickness).[26] The data are given in Table 3 and the correlation is shown in Fig. 8. Here the number of days to

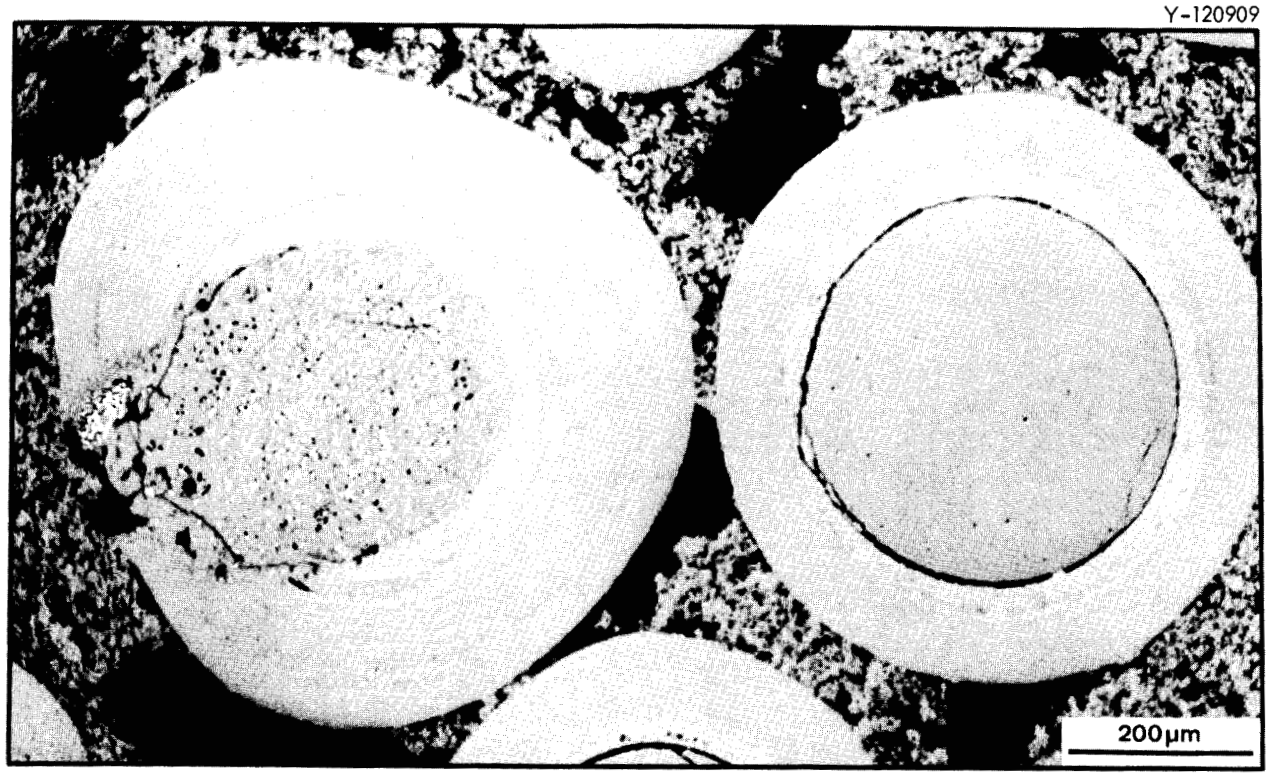

(4 Th, U)O_2 (8.3% FIMA) ThO_2 (0.3% FIMA)

Fig. 7. Typical Observation of Carbon Deposition and Oxide Kernel Migration Resulting from the Existence of a Temperature Gradient Across the Particle. The $Th_{0.8}U_{0.2}O_2$ particle was at an average temperature of 1405°C with a temperature gradient of 1250°C/cm, while the ThO_2 particle was at an average temperature of 1305°C with a temperature gradient of 1470°C/cm.

Table 3. Results of Experiments on Coating Failure in Urania Coated Particle Fuel of Dragon Reference Design[a]

Experiment	Average Particle Surface Temperature (°C)	Rating (W/particle)	Estimated Cross-Particle Temp. Difference (°C)	Irradiation Times and % FIMA at Onset of Failure	
				Days	% FIMA[b]
Riso LEHPD2 (Denmark)	1425	0.68	250	140	3.9
HTE (Dragon Reactor)	1650	0.26	125	85	0.91
HTE (Dragon Reactor)	1725	0.26	50	85	0.91
HTE (Dragon Reactor)	1900	0.26	125	8	0.085
Studsvik 16/1 (Sweden)	1650	1.4	280	10	0.58

[a]Data obtained from L. W. Graham.[26]

[b]Calculated assuming 800-μm-diam, fully dense UO_2 kernels and 3.1×10^{10} fissions W^{-1} sec^{-1}.

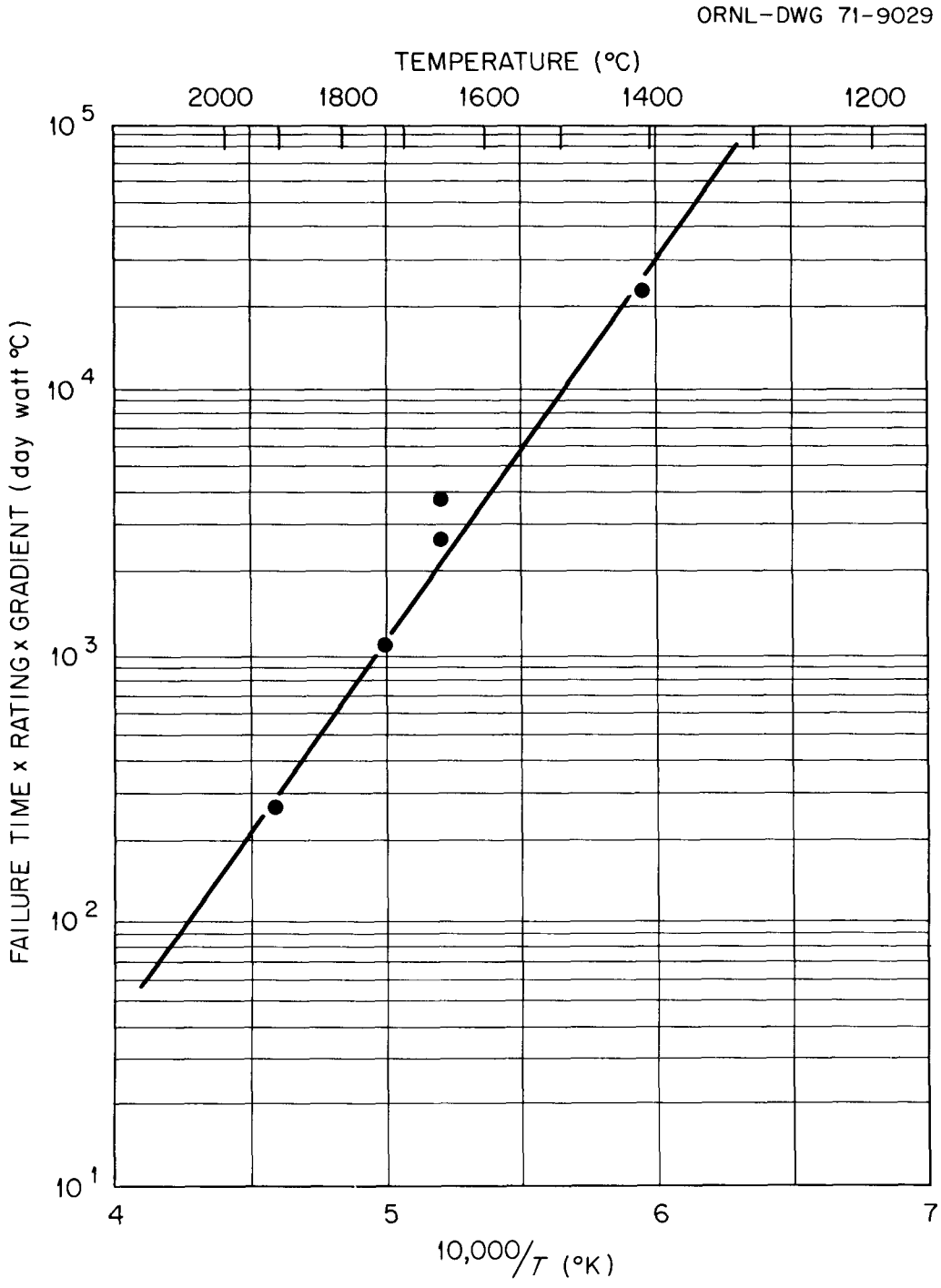

Fig. 8. Thermal Gradient, Power, and Temperature Dependence Determined by the Dragon Project for Fission Gas Release from Irradiated Urania Particles of the Dragon Project Reference Design.

failure was defined as the time to the initial rise in rate of release of noble gases, the gradient in temperature was that across the entire particle, and the rating had units of watts per particle. The usefulness of the Dragon Project correlation for fuels of the GGA design is not presently known. In view of the large differences between the two designs in burnup rate, enrichment, and volume within the particle for fission gas and carbon monoxide, it would seem fortuitous if the Dragon Project correlation would apply to U.S. particle designs.

4.2 First-Principle Derivations of Oxide Particle Transport Models

During operation of a reactor, temperature gradients are established across the oxide fuel particles. Such gradients may result in observable migration of carbon to the cold side of the particle and/or migration of the oxide kernel to the hot side of the particle. These observations lead one to propose cyclic processes such as the following to account for this behavior:

A. Reactions at the Hot Side

(1) CO_2 (arriving from the cold side) + C $\rightarrow$ 2CO

(2) [O] (in solid solution in the oxide) + C $\rightarrow$ CO

(3) C $\rightarrow$ [C] (in solid solution in the oxide)

B. Mass Transport Across the Temperature Gradient

(4) Solid-state diffusion of solid-solution oxygen through the oxide kernel.

(5) Gas-phase diffusion of CO and CO_2 through the porous buffer layer of carbon, the CO_2 diffusing from the cold to the hot side and the CO diffusing in the reverse direction.

(6) Solid-state diffusion of solid-solution carbon through the oxide kernel and down the temperature gradient.

C. Reactions at the Cold Side

(7) 2CO (arriving from the hot side) $\rightarrow$ CO_2 + C

(8) CO $\rightarrow$ [O] (in solution in the oxide) + C

(9) [C] (in solid solution in the oxide) $\rightarrow$ C.

In the above expressions the brackets indicate solid solution of a species. These mechanisms are interdependent and constitute several series or parallel sets. For example, if the series of processes (1), (5), and (7) were considered, as shown in Fig. 9, it can be seen that the slowest of the three would control mass transport. Another migration system is established by mechanisms (2), (4), and (8); again the slowest mechanism would control. Finally, the two sets of mechanisms operate in parallel, and the migration would be controlled at a particular temperature and temperature gradient by the set having the more rapid overall rate.

Derivations of the rates of specific mechanisms will be given below.

4.2.1 Calculated Rate of Carbon Transport by CO-CO_2 Diffusion

The carbon-transporting cycle shown in Fig. 9 is first assumed to be controlled by the rate of CO-CO_2 diffusion in the porous carbon buffer layer that immediately surrounds the kernel. Quantitative mathematical expressions for the carbon transport rate were derived (Appendix B) using the following assumptions about behavior within the particle:

(1) The total gas pressure at any point within the buffer layer is constant.

(2) Chemical equilibrium is maintained at each temperature within the buffer layer.

Gradients in P_{CO} and P_{CO_2} can be demonstrated to exist with the aid of Fig. 1. It can be seen that, at a given total $P_{CO} + P_{CO_2}$, the ratio

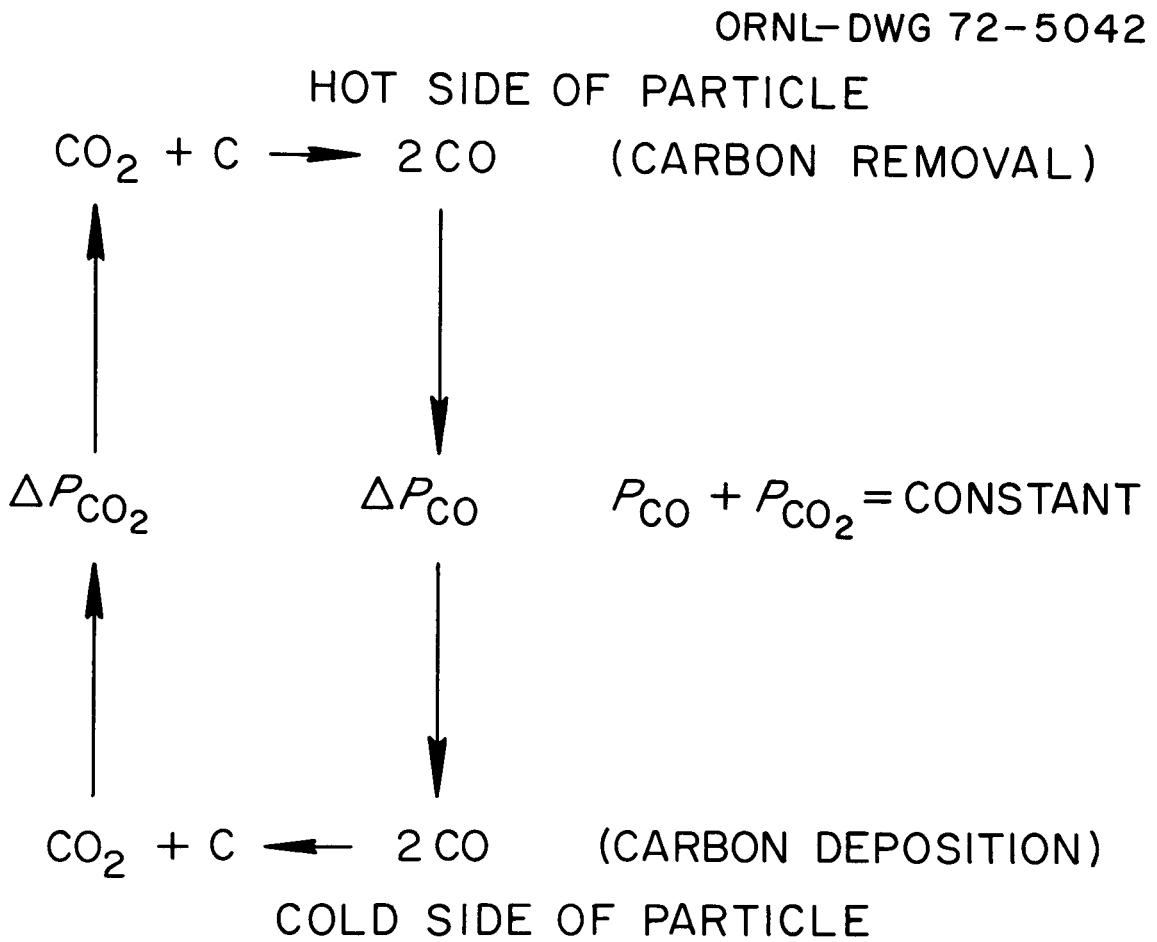

Fig. 9. Carbon-Transporting Cycle Postulated to Operate as a Result of CO-CO_2 Diffusion Within the Porous Buffer Coating of Oxide Coated Particles.

CO_2/CO decreases with increasing temperature. Therefore, carbon dioxide diffuses up and carbon monoxide diffuses down the temperature gradient, as shown in Fig. 9. The resulting expressions are summarized below:

Carbon Transport Out-of-Reactor (As-coated or Irradiated Particles). — The expression for carbon transport in out-of-reactor tests is derived in Appendix B, Eq. (B26), and is as follows:

$$y = \frac{\varepsilon'}{q'} kt \frac{dT}{dx} P_{CO} \frac{S_1}{S_2} , \qquad (2)$$

in which

y = micrometers (μm) of carbon transported,

$\frac{\varepsilon'}{q'}$ = ratio, observed diffusion coefficient to that in free space, dimensionless,

k = rate constant at a given $P_{CO} + P_{CO_2}$ and temperature for the $C-CO-CO_2$ system, μm of carbon hr^{-1} $(°C/cm)^{-1}$ atm^{-1}, Fig. B-1 (Appendix B),

t = time, hr,

x = general distance parameter, cm,

dT/dx = temperature gradient, °C/cm,

P_{CO}, P_{CO_2} = pressure of CO or CO_2, atm,

P_g = pressure of residual coating gases, usually 1 atm,

P_{fg} = pressure of Xe + Kr if present, atm,

S_1 = sum, $P_{CO} + P_{CO_2}$,

S_2 = sum, $P_{CO} + P_{CO_2} + P_g + P_{fg}$.

In-Reactor Carbon Transport Tests. — The transport equation for in-reactor tests will now be generally described. It appears that the oxygen

released in a particle (essentially as carbon monoxide) is not chemically buffered during burnup, as was discussed in Sect. 3.3. Thus, P_{CO} increases with burnup, as do the pressures of xenon and krypton. The mean-value-theorem is used in the transport equations to evaluate this change in pressure with burnup. The resulting equation for carbon transport at a given final burnup is derived in Appendix B, Eq. (B27), and is as follows:

$$y = \frac{\varepsilon'}{q'} k_\ell t \frac{dT}{dx} \frac{1}{F} \int_o^F \frac{P_{CO} S_1}{S_2 S_3} dF , \qquad (3)$$

in which

$$\log k_\ell = -7.837 + 9452/T$$

$$S_3 = \left(1 + \frac{2P_{CO_2}}{P_{CO}}\right)^2$$

F = percent FIMA.

Specific examples of the use of Eq. (3) will now be given. It is assumed that the release of oxygen, xenon, and krypton is linear with burnup, e.g., by using the ideal-gas law,

$$P_{CO} = \frac{m_{CO} R_1 TF}{a\Theta} + P_{CO} \text{ (initial)} , \qquad (4)$$

in which

m_{CO} = moles of oxygen released as CO per initial mole of U per percent FIMA,

R_1 = 82.06 cm^3-atm/mole-°K,

T = temperature, °K,

F = percent FIMA,

a = ratio (void volume in kernel and buffer layer/superficial volume of kernel),

Θ = molar volume of the fuel oxide, 24.6 cm^3/mole for UO_2.

Similar expressions are used for P_{CO_2} and $P_{(Xe + Kr)}$; it should be noted that the sum of m_{CO} and $2m_{CO_2}$ is equal to m, the total oxygen release per percent FIMA per mole of oxide.

Consider now the application of Eq. (3) to the irradiation of 93%-enriched UO_2 in HFIR (High Flux Isotope Reactor). Here typical burnup conditions are approximately 50 hr/% FIMA at a temperature gradient of approximately 200°C/cm. The BISO* particle is assumed to include a volume for fission gas that is three times the volume of the kernel (a = 3.0) and an initial P_{CO} of 1 atm. Two values of oxygen release per fission were used to correspond approximately with the high and low values calculated from the fission product yields; these values were 0.3 and 0.05 (see Tables 1 and 2). The results of these calculations at specific burnups for the two values of oxygen release are given in Figs. 10 and 11. It is immediately evident that the predicted carbon transport at full burnup is a centimeter or more even at $\varepsilon'/q' = 0.01$, where ε'/q' is the probable minimum ratio of the diffusion of gas in the buffer layer to that in free space. On the other hand, the transport necessary for particle failure is about 100 μm. Since these particles do not generally fail at full burnup, the predicted behavior is orders of magnitude greater than that normally observed.

Consider next the irradiation of ThO_2 particles. Here we assume 500 hr per % FIMA of ^{233}U in HFIR at a temperature gradient of 200°C/cm and a volume for fission gas that is equal to the kernel volume (a = 1.0). For one set of calculations that would give the maximum rate of carbon transport, we assumed P_{CO} = 1 atm initially and an oxygen release of 0.3 atom per

---

*BISO particle coatings consist of a low-density pyrolytic carbon layer and a high-density pyrolytic carbon layer.

ORNL-DWG 73-5073R

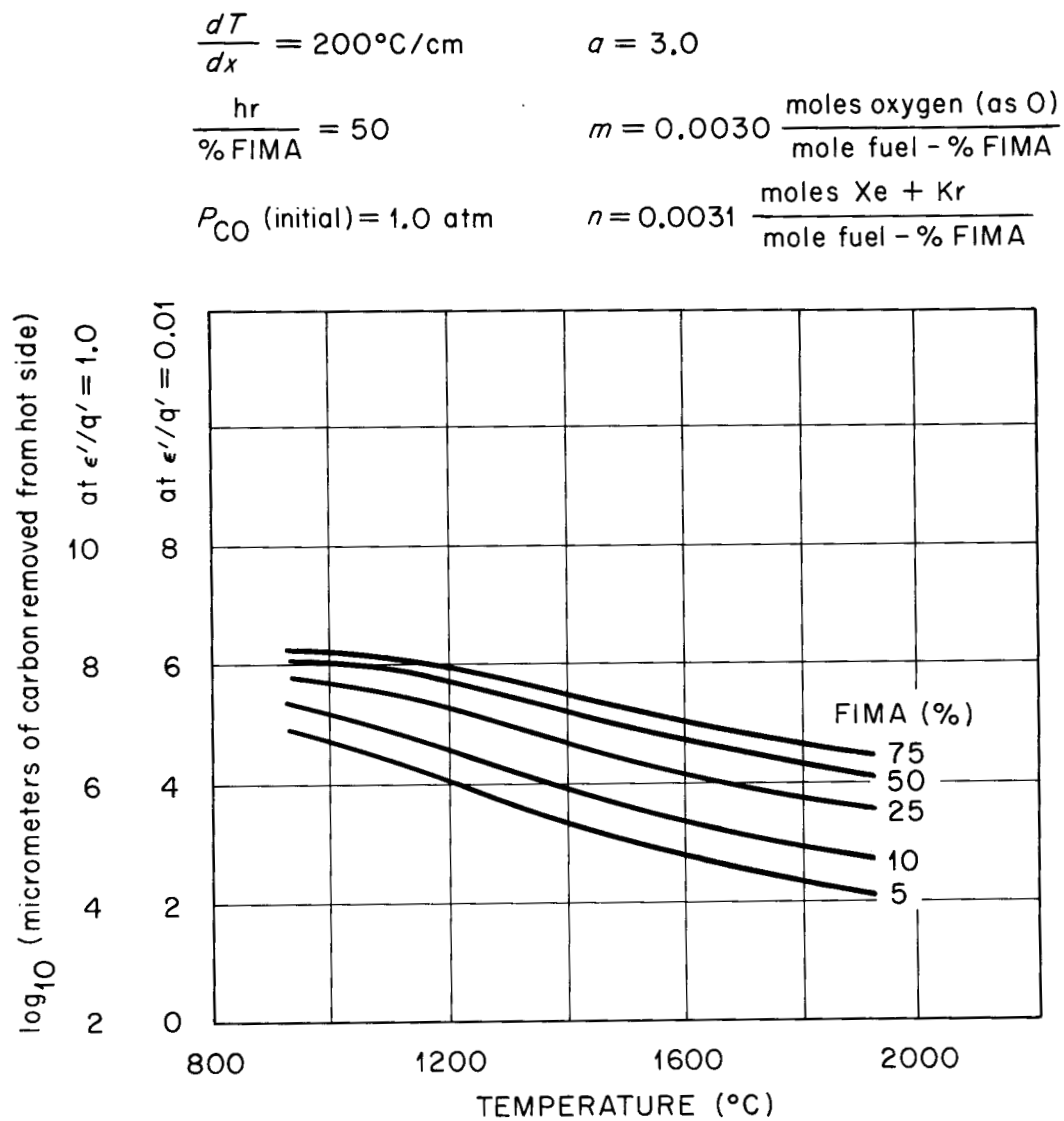

Fig. 10. Carbon Transport Calculated to Occur via CO-CO_2 Interdiffusion in BISO-Coated UO_2 Particles at Typical HFIR Conditions for Burnup Rate and Temperature Gradient. The assumed oxygen release is 0.3 atom per fission.

ORNL-DWG 73-5072R

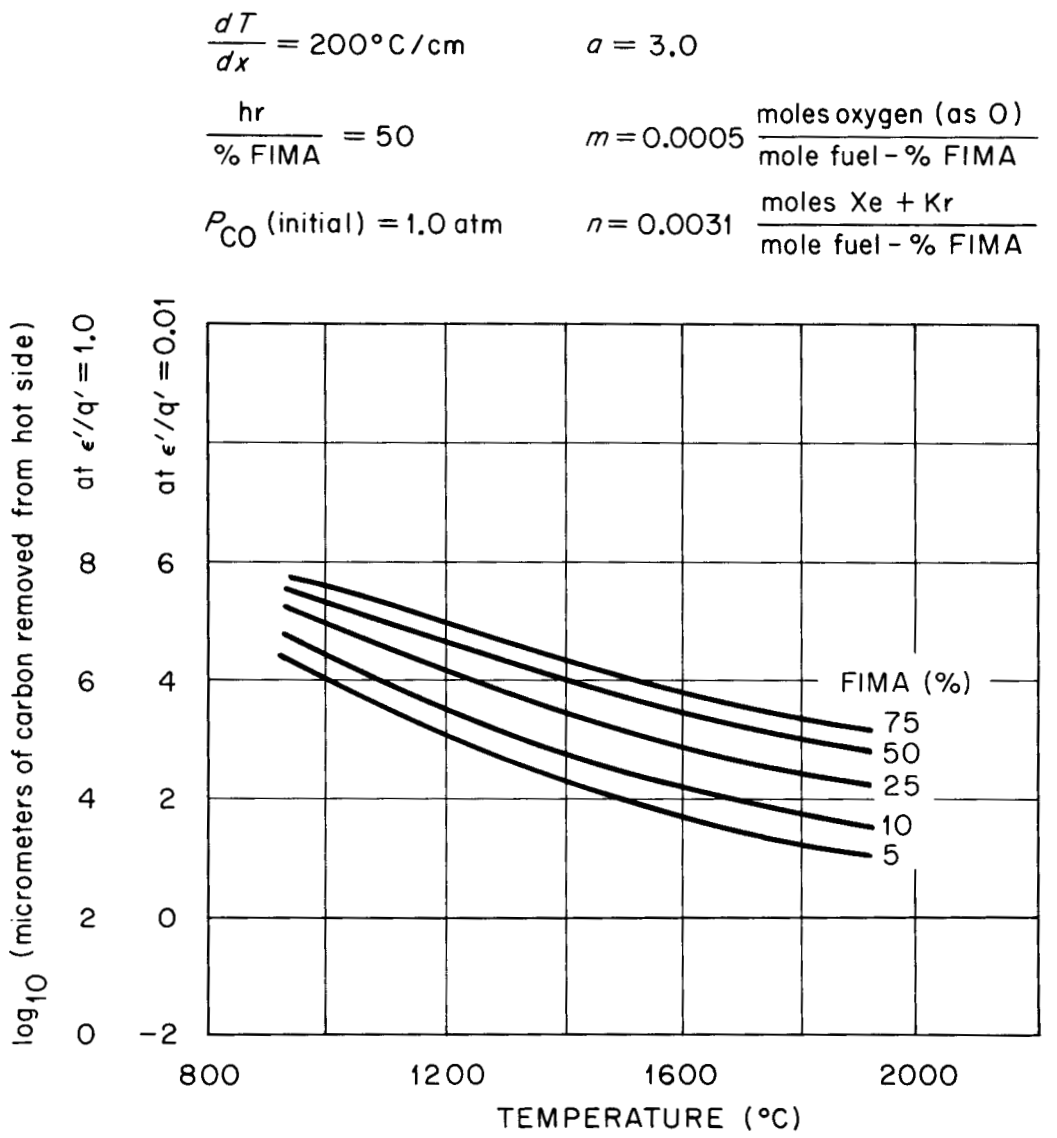

Fig. 11. Carbon Transport Calculated to Occur via $CO-CO_2$ Interdiffusion in BISO-Coated UO_2 Particles at Typical HFIR Conditions for Burnup Rate and Temperature Gradient. The assumed oxygen release is 0.05 atom per fission; the other parameters are the same as those in Fig. 10.

fission; the results are given in Fig. 12. For the calculation of the minimum transport we assumed P_{CO} = 0.001 atm initially and an oxygen release of 0.05 atom per fission. Again, the predicted transport (see Fig. 13) is several orders of magnitude larger than the observed transport in irradiated BISO-coated ThO_2 particles.

The discrepancy between values predicted by the gas-phase transport theory and those obtained in actual practice apparently cannot be rectified at the present time. Experience with the sensitivity of the various numerical parameters in the mathematical model indicates that the only possible way that the calculated carbon transport rates could be made to agree with the observed rates would be to have an extraordinarily low value of 10^{-5} for ε'/q' or an oxygen release per fission of approximately 0.005 (m = 0.00005) or less. The latter value is inconsistent with those given in Tables 1 and 2.

4.2.2 Calculated Rate of Carbon Transport Controlled by Carbon Monoxide Disproportionation

Consider the rate of the reaction

$$2CO \rightarrow CO_2 + C$$

at the cold side of the particle to be controlling the rate of the carbon transport cycle shown in Fig. 9. Data from only two studies relative to the rate of this reaction in the absence of catalysts are known to exist. Both studies were carried out at temperatures and pressures considerably lower than those in oxide particles in the HFIR; thus our extrapolations of these data may give erroneous results. This reaction is reported by Reif[34] to be proportional to P_{CO} with an activation energy of 13,200 cal/mole, while Pursley et al.[35] found the reaction rate to be zero order

ORNL-DWG 73-5071R

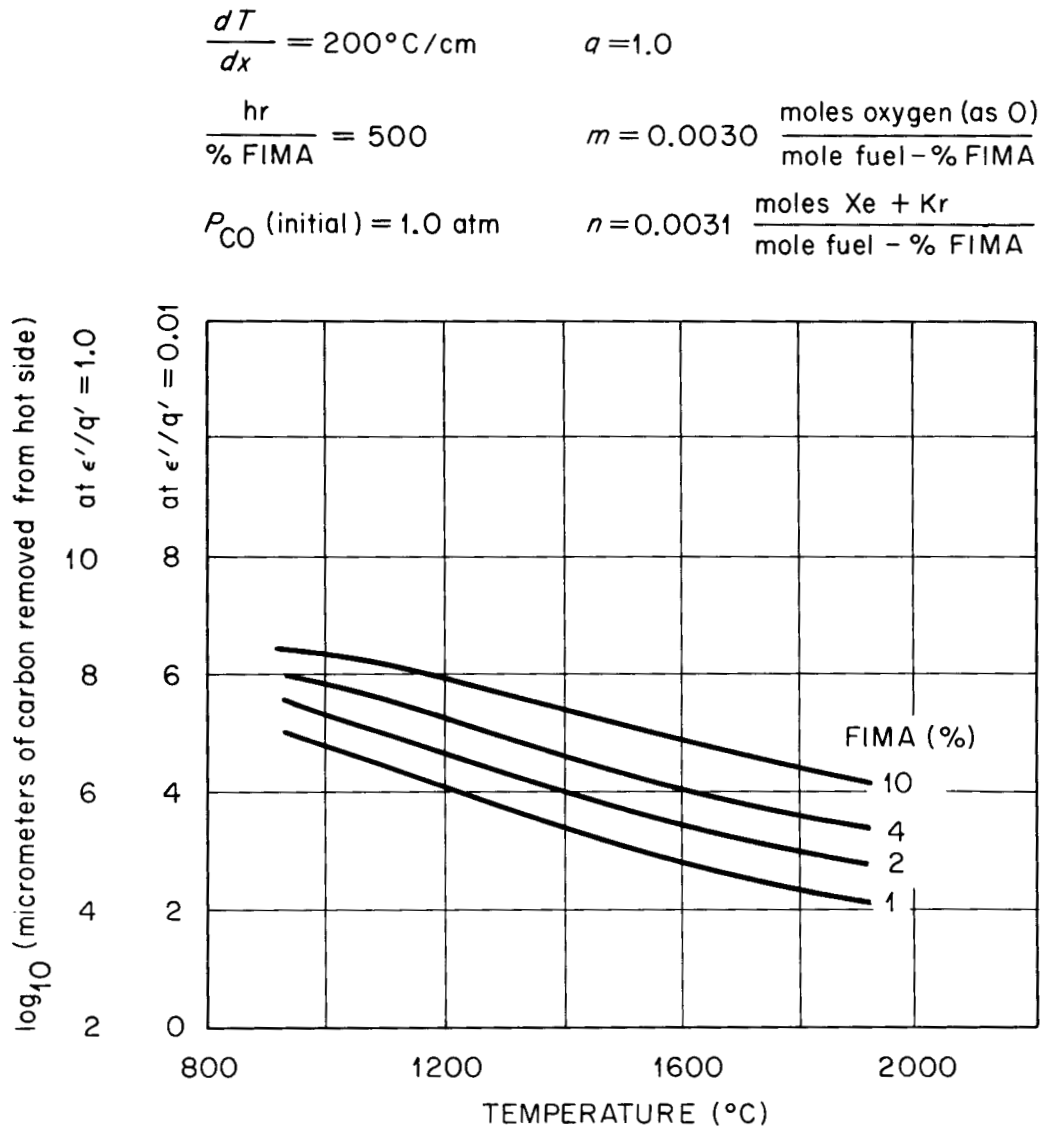

Fig. 12. Carbon Transport Calculated to Occur via $CO-CO_2$ Interdiffusion in BISO-Coated ThO_2 Particles at Typical HFIR Conditions for Burnup Rate of ^{233}U and Temperature Gradient. The assumed oxygen release is 0.3 atom per fission and P_{CO} (initial) is 1.0 atm.

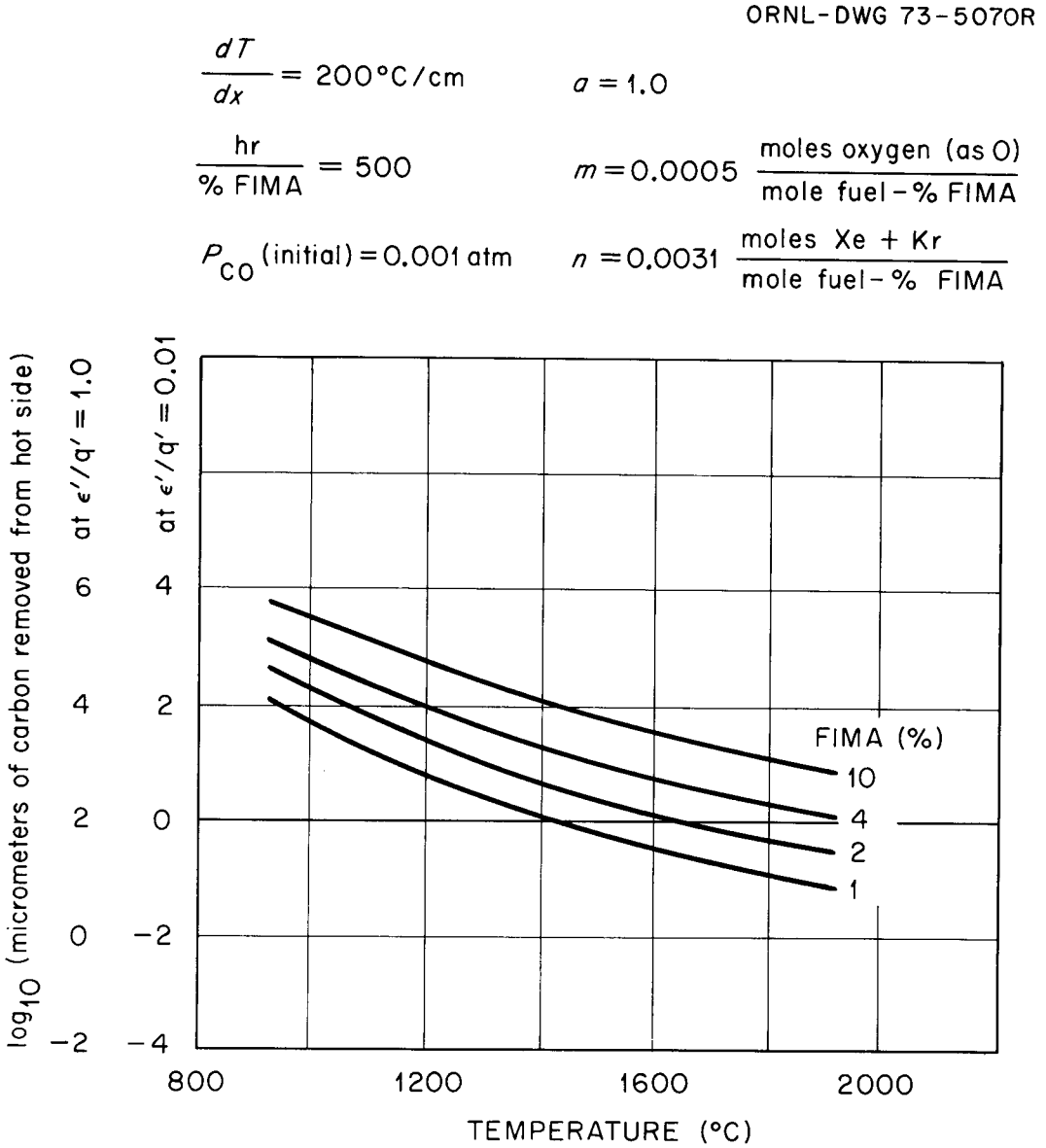

Fig. 13. Carbon Transport Calculated to Occur via $CO-CO_2$ Interdiffusion in BISO-Coated ThO_2 Particles at Typical HFIR Conditions for Burnup Rate of ^{233}U and Temperature Gradient. The assumed oxygen release is 0.05 atom per fission and P_{CO} (initial) is 0.001 atm; the other parameters are the same as those in Fig. 12.

with an activation energy of 35,900 cal/mole. The rate also appears to be dependent on the surface/volume ratio (S/V) of the carbon in which the decomposition of carbon monoxide is occurring.[34,35] Consequently, one must keep these reservations in mind in the following application of the data to the oxide particle system. Lackey[36] has measured S/V in the buffer layer carbon in unirradiated ThO_2 coated particles and found it to be about 12 m^2/cm^3. If one assumed a 100-μm-thick buffer layer (ℓ_B) and only 2 m^2/cm^3 for the S/V ratio, then the amount of carbon removed from the hot side of a particle as a result of the carbon deposition at the cold side in-pile (with Reif's[34] data) would be:

$$y = 0.0021 \exp\left(\frac{-13,200}{RT}\right) t\ell_B \frac{S}{V} \frac{1}{F} \int_o^F P_{CO}\, dF , \qquad (5)$$

in which t, y, and F retain the same units as used previously. By using the ideal-gas law for P_{CO} and substituting for ℓ_B and S/V, integration of Eq. (5) gives:

$$y = 0.42 \exp\left(\frac{-13,200}{RT}\right) \left(\frac{t}{F}\right) \left(\frac{mRT}{2a\Theta} F^2 + P_{CO}(\text{initial})\, F\right) . \qquad (6)$$

This latter equation has been used to calculate the results shown in Fig. 14 for burnup of UO_2 in the HFIR. Again, the calculated amount of carbon transported is orders of magnitude greater than that observed. Use of Pursley's[35] P_{CO}-independent rate data results in an equation in which y is proportional to time; use of this equation gave results which generally did not differ in magnitude from those shown in Fig. 14. The rates for the hot-side reaction, $CO_2 + C \rightarrow 2CO$, were also considered, but these rates were always faster than those for the CO-disproportionation reaction. Thus

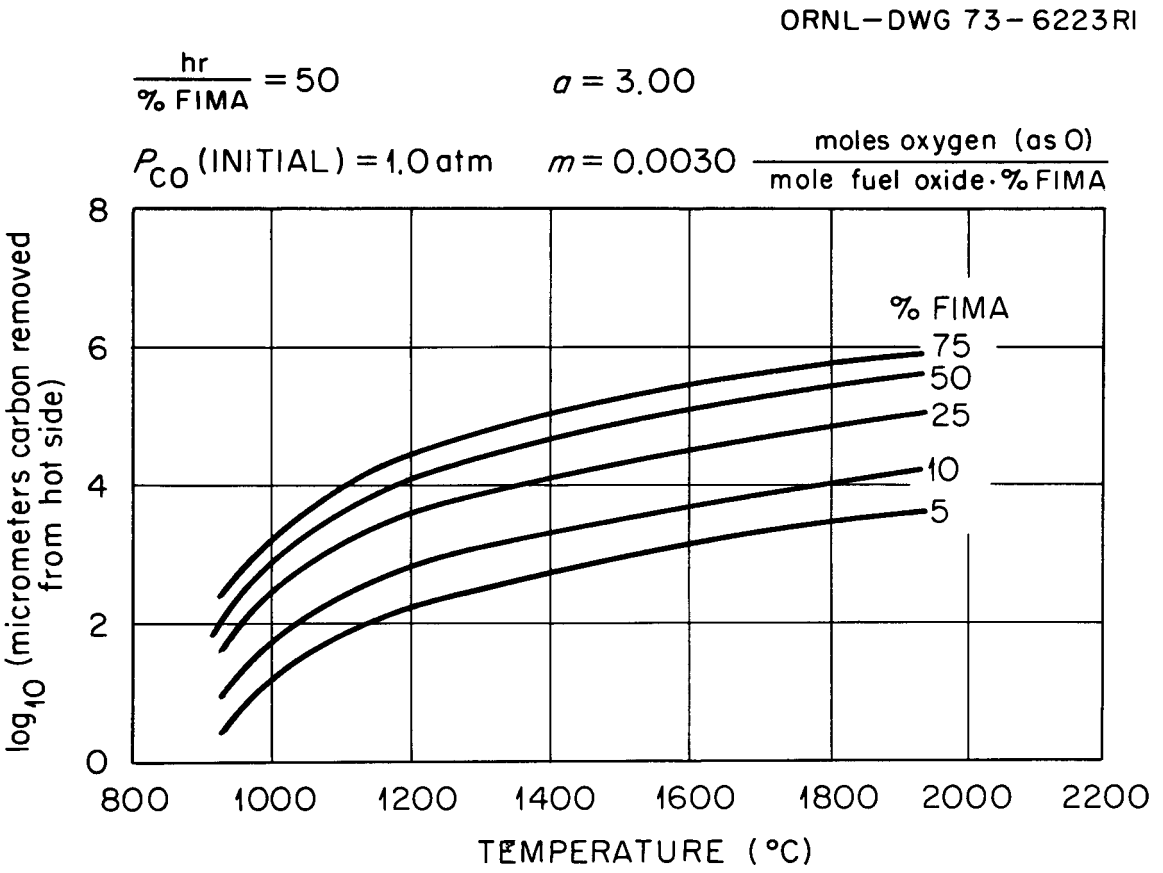

Fig. 14. Carbon Removal from Hot Side of Particle Calculated to Occur at Typical HFIR Conditions in BISO-Coated UO_2 Particles as a Result of Rate Control by the CO-Decomposition Reaction Within the Buffer Layer on the Cold Side of a Coated Particle.

it again appears that the predictions of theory are at considerable variance with practice and that no definitive identification of the rate-controlling mechanism for transport in oxide fuels can yet be made. However, if we take the calculations made thus far at face value, then a comparison of the calculated results in Fig. 10 for gas-phase interdiffusion with those in Fig. 14 indicates that the decomposition rate of carbon monoxide at T < about 1400 to 1500 °K would result in the removal of less carbon than that resulting from gas-phase transport and hence would appear to be controlling below these temperatures. Another important effect not considered here is catalysis of the reaction by the fission product elements; this effect could either accelerate or retard the reaction.

4.2.3 Rate of Carbon Deposition or Kernel Migration by Solid-State Diffusion Mechanisms

The analysis of solid-state mass transport through an oxide kernel would appear to be similar to that developed for dicarbides by Gulden.[31] His analysis suggests that the equation for the flux of rate-controlling species j through an oxide kernel would be:

$$J_j = -\frac{C_j D_j^*}{RT}\left[\frac{d\mu_j}{dT} - \frac{(\mu_j - Q_j^* - \bar{h}_j)}{T}\right]\frac{dT}{dx} , \qquad (7)$$

in which

C_j = concentration of species j in the oxide, moles/cm^3,

D_j^* = self-diffusion coefficient in the oxide of species j, cm^2/sec,

$\bar{h}_j$ = heat of solution (partial molal enthalpy) of species j, cal/mole,

μ_j = chemical potential of species j, cal/mole,

Q_j^* = heat of transport of species j in the kernel, cal/mole.

In the event that solid-state diffusion was established as the rate-controlling mechanism, the identification of the rate-controlling species, j, would be necessary for the application of Eq. (7). For the purpose of illustration, let us assume that this species was solid-solution oxygen [O]. Since $\mu_{[O]} = \mu_{O_2} = RT \ln P_{O_2}$, and assuming that the local oxygen potential of the oxide kernel in a temperature gradient was maintained at that for the local equilibrium

$$2C + O_2 \rightleftarrows 2CO \ , \tag{8}$$

it can readily be demonstrated that

$$\frac{d\mu_{[O]}}{dT} - \frac{\mu_{[O]}}{T} = \frac{-\Delta H_1^\circ}{T} \ , \tag{9}$$

in which

ΔH_1° = standard enthalpy of reaction (8). Thus,

$$J_{[O]} = \frac{C_{[O]} D^*_{[O]}}{RT^2} \left[\Delta H_1^\circ + \bar{h}_{[O]} + Q^*_{[O]} \right] \frac{dT}{dx} \ . \tag{10}$$

A paper by Aitken[37] provides values of $\bar{h}_{[O]}$ and also treats thermal diffusion in oxide fuels more extensively than was done here. Application of Eq. (10) to a fissioning system would also need, in principle, to include the experimental variation of factors such as $Q^*_{[O]}$, $D^*_{[O]}$, and $\bar{h}_{[O]}$ with fission.

4.3 Theoretical Basis for Correlation of Irradiation Data

The equations derived in Sect. 4.2 for calculating transport behavior in oxides can be used to derive relationships for correlation of experimental data similar to that used for carbide particles[31-33] or by the Dragon Project (Fig. 8). This method provides a possible means for

obtaining useful correlations from experimental observations without having to know all the quantities specified in the first-principle derivations. Such an approach was used in calculating the kernel migration coefficient for carbides.[31-33] The derivations to be made below for P_{CO}-dependent mechanisms result from mathematical simplifications of the exact derivations under the following conditions: (a) P_{CO} (after fission) > about 4 P_{CO} (initially), (b) $P_{CO} > 0.1\ P_{CO_2}$, (c) $P_{CO} + P_{fg} > P_g$, (d) P_{CO} increases linearly with fission.

Consider first the derivation of an experimental correlation from the model for diffusion of CO and CO_2 in fission gas, Eq. (3). By using the assumptions above and the ideal gas law for calculation of P_{CO} and P_{fg}, it can be shown that Eq. (3) can be expressed in the form

$$y \approx (\text{constant}) \frac{dT}{dx} \frac{T}{a} \frac{t}{F} \int_0^F F\, dF \quad . \tag{11}$$

Integration of this equation indicates that y is proportional to F^2, as is generally indicated in Figs. 10-13 for the exact application of Eq. (11) (e.g., increasing F by a factor of 10 increases y by a factor of 100). Since F^2 can be written as $(F/t)^2\ t^2$, Eq. (11) can be put in the form

$$y = \alpha_1 \frac{dT}{dx} \frac{T}{a} \frac{F}{t} t^2 \tag{12a}$$

or

$$\frac{\frac{y}{t} a}{Tt \frac{dT}{dx} \frac{F}{t}} = \alpha_1 \quad . \tag{12b}$$

The terms in α_1 can be shown to be:

$$\alpha_1 = \frac{\varepsilon'}{q'} k_\ell \frac{m^2}{(m+n)} \frac{R}{\Theta} . \tag{13}$$

As long as α_1 can be assumed to be time- and fission-independent, to follow a single mechanism over all temperatures, and to obey the Arrhenius relation, then a plot of log α_1 vs 1/T should be linear if the gas-phase interdiffusion mechanism is rate-controlling in the experimental system. Note that k_ℓ, Eq. (B23) in Appendix B, does satisfy this requirement. In Eq. (12b) it should be noted that y/t is the observed time-averaged transport rate and F/t is proportional to the power generated in a fully dense kernel.

The equations for rate control by the decomposition of carbon monoxide can be treated in the same manner. For the condition that the rate is proportional to P_{CO} [Eq. (5)], it can be readily demonstrated that

$$y = \alpha_2 \frac{T}{a} \frac{F}{t} t^2 \tag{14a}$$

or

$$\frac{\frac{y}{t} a}{Tt \frac{F}{t}} = \alpha_2 \tag{14b}$$

while, for the case in which the rate is P_{CO}-independent, one obtains

$$y = \alpha_3 t \tag{15a}$$

or

$$\frac{y}{t} = \alpha_3 . \tag{15b}$$

The correlations for rate control by a solid-state diffusion mechanism can be deduced from two limiting cases for Eq. (7). If $|d\mu_j/dT| \ll |\mu_j - Q_j^* - \bar{h}_j|$, then the correlation would apparently take the form[31]

$$y = \alpha_4 \frac{t}{T^2} \frac{dT}{dx} \tag{16a}$$

or

$$\frac{\frac{y}{t} T^2}{\frac{dT}{dx}} = \alpha_4 \quad . \tag{16b}$$

On the other hand, if the absolute values of these quantities had the opposite sense, then the correlation would apparently be

$$y = \alpha_5 \frac{t}{T} \frac{dT}{dx} \tag{17a}$$

or

$$\frac{\frac{y}{t} T}{\frac{dT}{dx}} = \alpha_5 \quad . \tag{17b}$$

The term α_4 has been called the "kernel migration coefficient;"[31] this terminology will be used here also. Again, as long as the rate equations leading to the derivations of the coefficients α_2 through α_5 can each be based on a single mechanism operating over a given temperature range, then each coefficient can be plotted vs 1/T as long as the simple Arrhenius behavior is obeyed.

4.4 Methods for Determination of the Rate-Controlling Mechanism

The mathematical equations presented above for the prediction of

migration rates can possibly be used to determine which of the many mechanisms is actually rate-controlling. In both in-reactor and out-of-reactor experiments, an array of particles exists in either a fuel rod or in an experimental particle holder; depending upon the particle position within the array, each particle is subjected to a reasonably well-known temperature and temperature gradient. Also, the migration or transport in each particle can be measured by standard radiographic or metallographic techniques. The latter measurements can then be used to calculate the ratio of observed transport in a particle located at any position within the array to that for a particle at, conveniently, the midpoint of the array. Such a ratio can also be calculated from the mathematical equations and has the great advantage of the cancellation of such unknown parameters as ε'/q', S/V, etc. Even if the parameters vary with fission or time, their ratio is still unity, since all particles experience the same time and fission.

For CO-CO_2 interdiffusion, the ratio is obtained from Eqs. (2) and (3) and at $T > 1250°K$ can be shown to be:

$$\frac{y_x}{y_{\bar{x}}} = 10^{+9452\tau} \frac{\left(\frac{dT}{dx}\right)_x}{\left(\frac{dT}{dx}\right)_{\bar{x}}} \alpha \quad , \tag{18}$$

in which

$$\bar{x} = 0.5\ (x_{max} + x_{min}),$$

$$\tau = \left(\frac{1}{T_x} - \frac{1}{T_{\bar{x}}}\right),\ T \text{ in } °K,$$

$$\alpha = \frac{T_x}{T_{\bar{x}}} \text{ for unirradiated particles;}$$

and in irradiated particles in which gas pressures vary with burnup,

$$\alpha' = \frac{\left[\int_o^F \frac{P_{CO}S_1}{S_2S_3}\,dF\right]_x}{\left[\int_o^F \frac{P_{CO}S_1}{S_2S_3}\,dF\right]_{\bar{x}}} \approx 10^{-0.002(T_x - T_{\bar{x}})} \; . \qquad (19)$$

The value of α' for irradiated particles increases by about a factor of 2 as temperature decreases by about 150°C (see Figs. 10-13); however, since this is only an approximation and is a relatively small effect, the value of α for unirradiated particles was used in the present calculations. These equations were used to calculate the indicated ratios shown in Fig. 15 for a typical in-pile experiment and in Fig. 16 for a typical out-of-pile experiment.

For rate control by the CO-decomposition reaction, the ratio is obtained from Eq. (6) and for P_{CO}(initial) << P_{CO}(from fission) is

$$\frac{y_x}{y_{\bar{x}}} = \alpha \exp\left(-\frac{13,200}{R}\,\tau\right) \; . \qquad (20)$$

This equation was used to calculate the ratios shown in Figs. 15 and 16 for an activation energy of either 13,200 cal/mole from Reif[34] or 35,900 cal/mole from Pursley et al.[35]

For rate control by a solid-state diffusion mechanism, Eq. (16a) was assumed to obey the Arrhenius relation and was arranged to give

$$\frac{y_x}{y_{\bar{x}}} = \frac{\left(\frac{dT}{dx}\right)_x \exp\left(-\frac{Q}{R}\,\tau\right)}{\left(\frac{dT}{dx}\right)_{\bar{x}} \alpha^2} \; . \qquad (21)$$

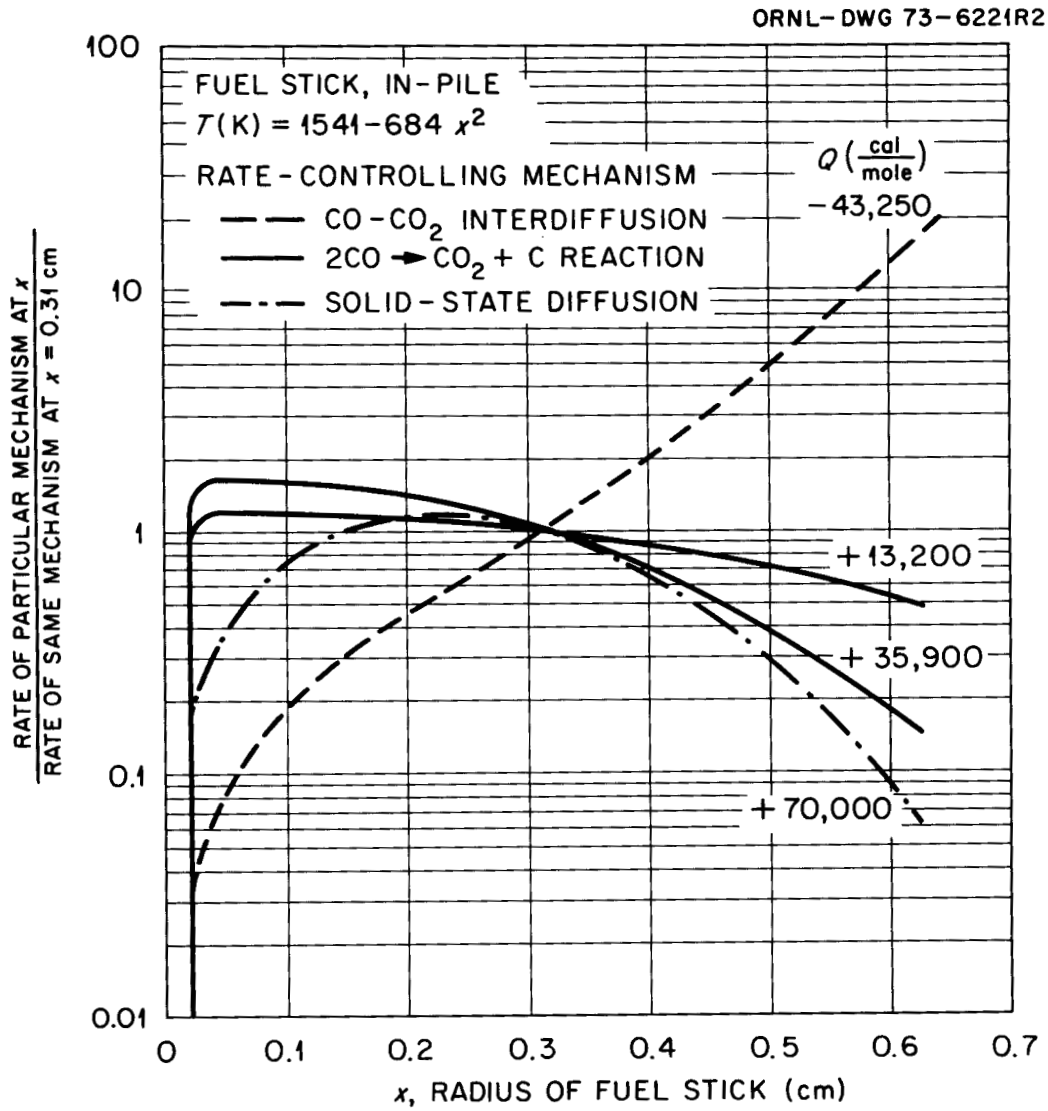

Fig. 15. Calculated Ratio of Transport Behavior Resulting from Rate Control by Indicated Mechanisms in BISO-Coated Oxide Particles Irradiated in a Fuel Rod.

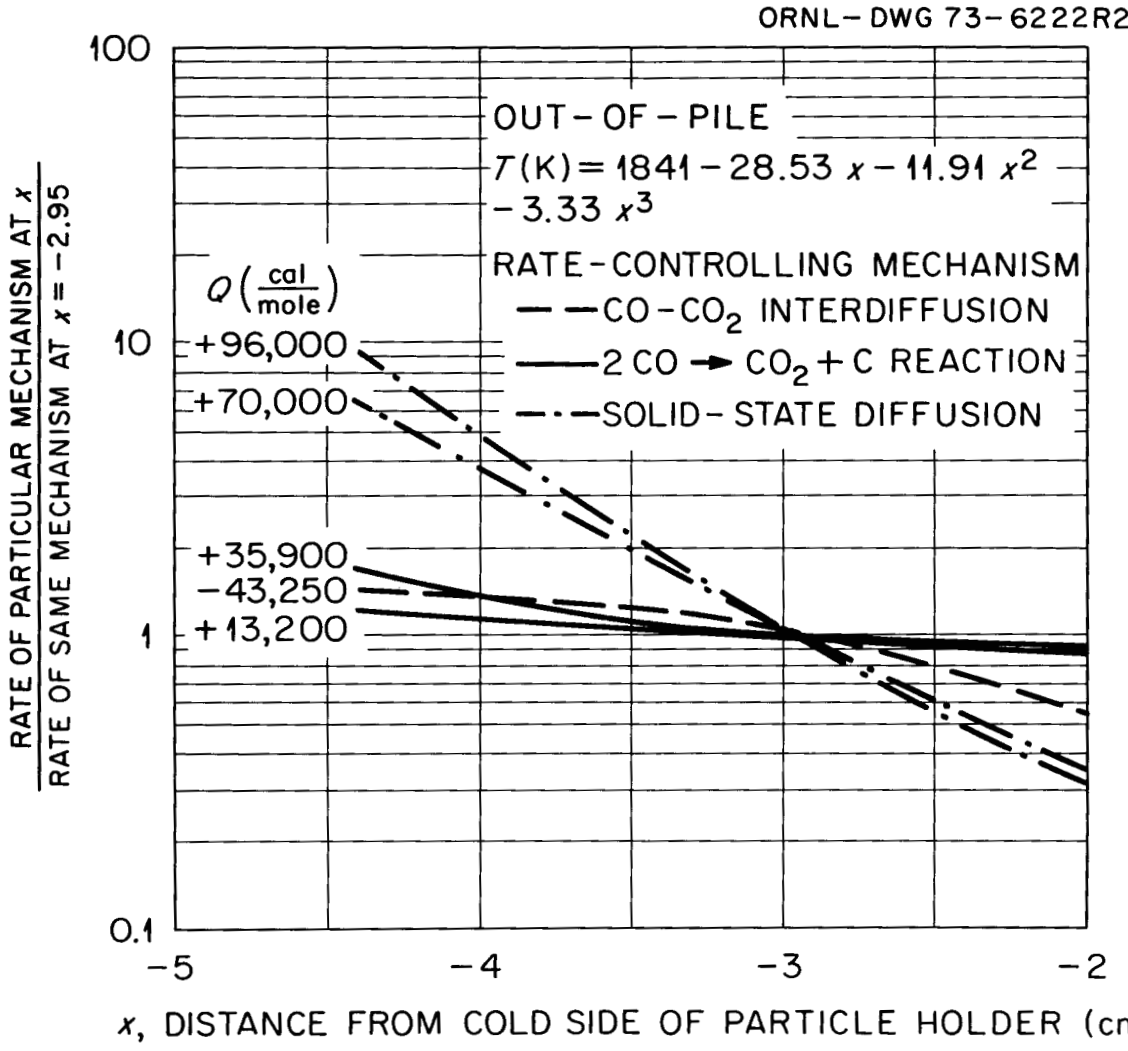

Fig. 16. Calculated Ratio of Transport Behavior Resulting from Rate Control by Indicated Mechanisms in BISO-Coated Oxide Particles When Heated in a Typical Laboratory Furnace. These results apply to either as-coated or irradiated particles.

This equation was used to calculate the ratios shown in Figs. 15 and 16 for an activation energy, Q, of either 70,000 or 96,000 cal/mole, these values being typical for solid-state diffusion.

A comparison of the calculated results in Figs. 15 and 16 can now be made. As shown in Fig. 15, the temperature in a fuel rod decreases with increasing radius while the temperature gradient increases from zero at the center of a fuel rod to, in this example, 267°C/cm at the surface. It is immediately evident that, for this condition, rate control by the CO-CO_2, gas-phase diffusion mechanism would give a ratio markedly different from ratios resulting from control by other mechanisms. The particles at or within 0.15 cm of the outer surface of the fuel rod should show much more transport than those in the interior. On the other hand, control by either a gas-solid reaction or a solid-state diffusion mechanism would result in particles showing the maximum transport at or within approximately midradius. In the out-of-reactor experiments (Fig. 16), both the temperature and the temperature gradient decrease with increasing distance, an effect just opposite to that in a fuel rod. Control by solid-state diffusion is the mechanism having a rate behavior that is considerably different from the other mechanisms, as long as the activation energy is as high as those shown in Fig. 16.

Thus, the combination of in-reactor and out-of-reactor experiments conceivably will permit the identification of the rate-controlling mechanism. Application of this technique does require that the scatter in the experimental behavior be within a factor of $\pm\sqrt{10}$ and consistency of mechanical properties such as the thermal conductivity of the binding matrix and uniformity of particle-matrix thermal contact. Once this is

accomplished, then the theoretical and experimental programs can more justifiably concentrate on the first-principle quantification of the rate data.

One obvious problem with the experimental application of these techniques is the inability to measure the extent of gas-phase carbon transport. It is conceivable that coating failure as a pressure vessel could occur by this process without metallographically observable effects. Occurrence of failure would need to be measured by an indirect technique such as release of fission gas, as was done in the Dragon Project experiments,[26] or observation of partial conversion of the oxide kernel to carbide. Nevertheless, once adequate measurement techniques are developed, then the resulting data may be treated by the methods described here.

4.5 Analysis of Experimental Data

The analytical methods described above will now be applied to the analysis of kernel migration in an irradiated fuel rod designated as H-1-2. This rod was part of a set of recent irradiation experiments that have provided a large amount of data for kernel migration in BISO particles containing UO_2, ThO_2, $Th_{0.8}U_{0.2}O_2$, or $Th_{0.67}U_{0.33}O_2$; these experiments are described extensively elsewhere.[38] Generally, the particles in these experiments were placed in 1.27-cm-diam fuel rods having a matrix made from a carbonized pitch-carbon mixture. The specific characteristics of fuel rod H-1-2 are listed in Table 4.

The temperature equation in Table 4 needs some explanation. Carslaw and Jaeger[39] derived the equation for radial temperature dependence under the conditions of uniform heat generation and a constant thermal

conductivity, K_{th}, within an infinitely long cylinder of radius r_r. If one converts their definition of the rate of heat generation (in watts per cm^3) to watts per cm of length, q, then this equation takes the form

$$T = a_o - a_2 x^2 \quad , \tag{22}$$

in which

a_o = fuel rod center-line temperature, °K,

$a_2 = q/4\ \pi K_{th} r_r^2$, °K/cm^2,

$0 \leq x \leq r_r$.

Equation (22) will be used in the analysis of the H-1-2 experiment; if one were to consider the minor effects of axial holes within the fuel rod or the temperature dependence of K_{th}, then derivations such as those given by Robertson[40] would be useful.

Table 4. Characteristics of Fuel Rod H-1-2

Temperature equation	$T(°K) = 1523 - 893x^2$
Particle type	BISO-coated UO_2 (93% enriched)
Kernel diameter, μm	114
Void ratio, a	3.09
Burnup, % FIMA	29.6
Duration of exposure, days	97.1

The extent of the migration of the hot-side kernel-carbon interface in individual particles was measured from a 100X photo-composite of radial cross sections. This migration was simply defined as the difference between the postirradiation separation of this interface from some convenient reference interface (such as the buffer carbon—dense carbon interface or the surface of the particle) and the original, preirradiation separation of these same interfaces; the latter locations were readily discernible in the photo-composites. No corrections were made to these measurements to compensate for geometric effects originating from elongation of the kernels during irradiation and for the fact that the plane-of-polish is not at the particle equator. A second set of measurements gave the location of the front and back of the particle-matrix interface with respect to the center of the fuel rod; the average of these two measurements is thus the radial location within the fuel rod of the center of the particle. The data obtained by these techniques are given in Fig. 17.

This latter plot along with one calculated from first principles, Fig. 18, was used to demonstrate that $CO-CO_2$ diffusion is not the rate-controlling mechanism for kernel migration. Figure 18 was prepared by utilizing Eqs. (18)—(21) and the temperature equation in Table 4. Comparison of the calculated and experimental data strongly suggests that $CO-CO_2$ diffusion does not control the kernel migration rate. Control by $CO-CO_2$ diffusion would result in maximum kernel migration at the surface of the fuel rod; it can be seen in Figs. 17 and 18 that the maximum migration occurs from about one-third of the fuel-rod radius to the surface of the rod. Similar plots were also made for particles in other fuel rods in the H-1 and H-2 experiments; again, the data suggest that $CO-CO_2$ diffusion does not control the rate of kernel migration.

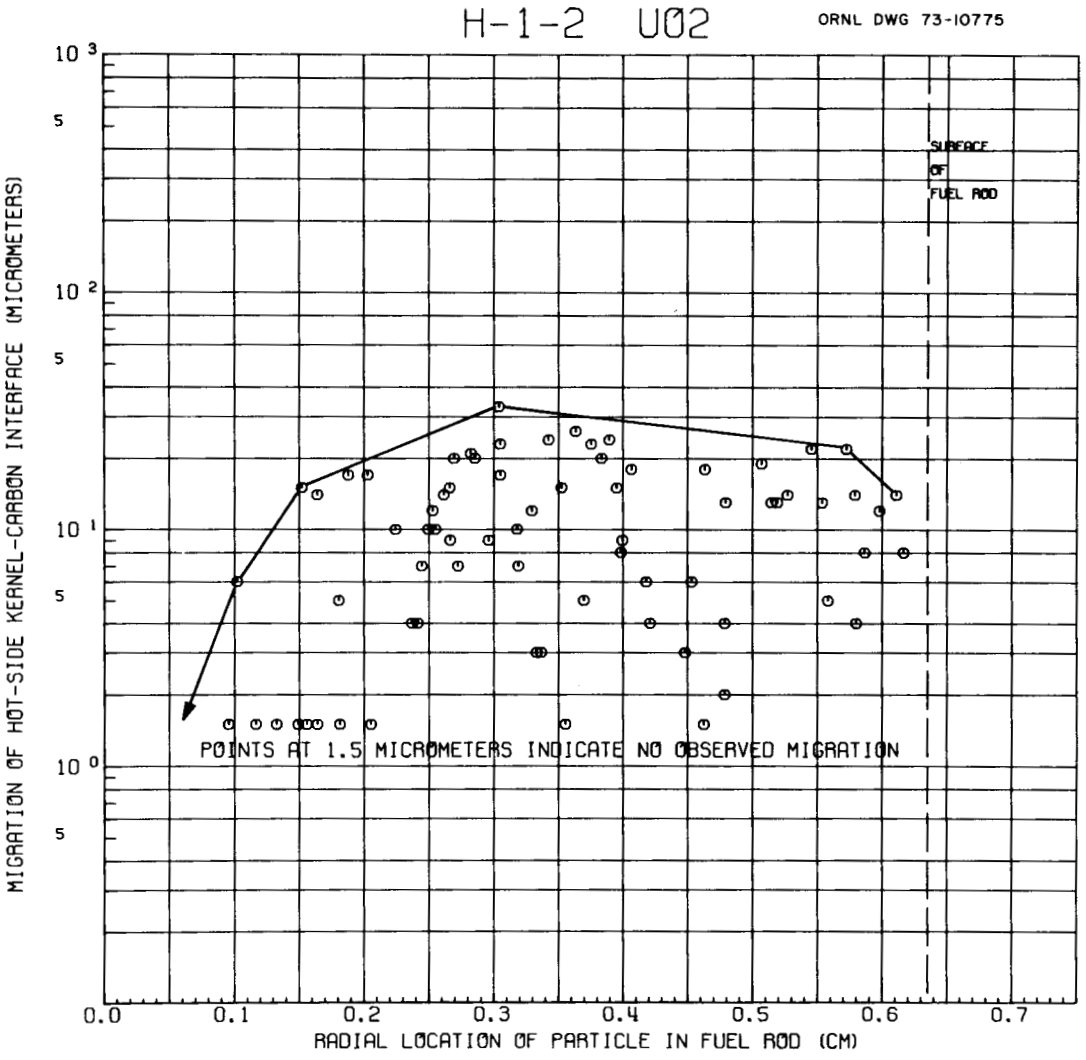

Fig. 17. Experimental Observation of Kernel Migration in BISO-Coated UO_2 Particles in Fuel Rod H-1-2 vs Radial Location of Particles.

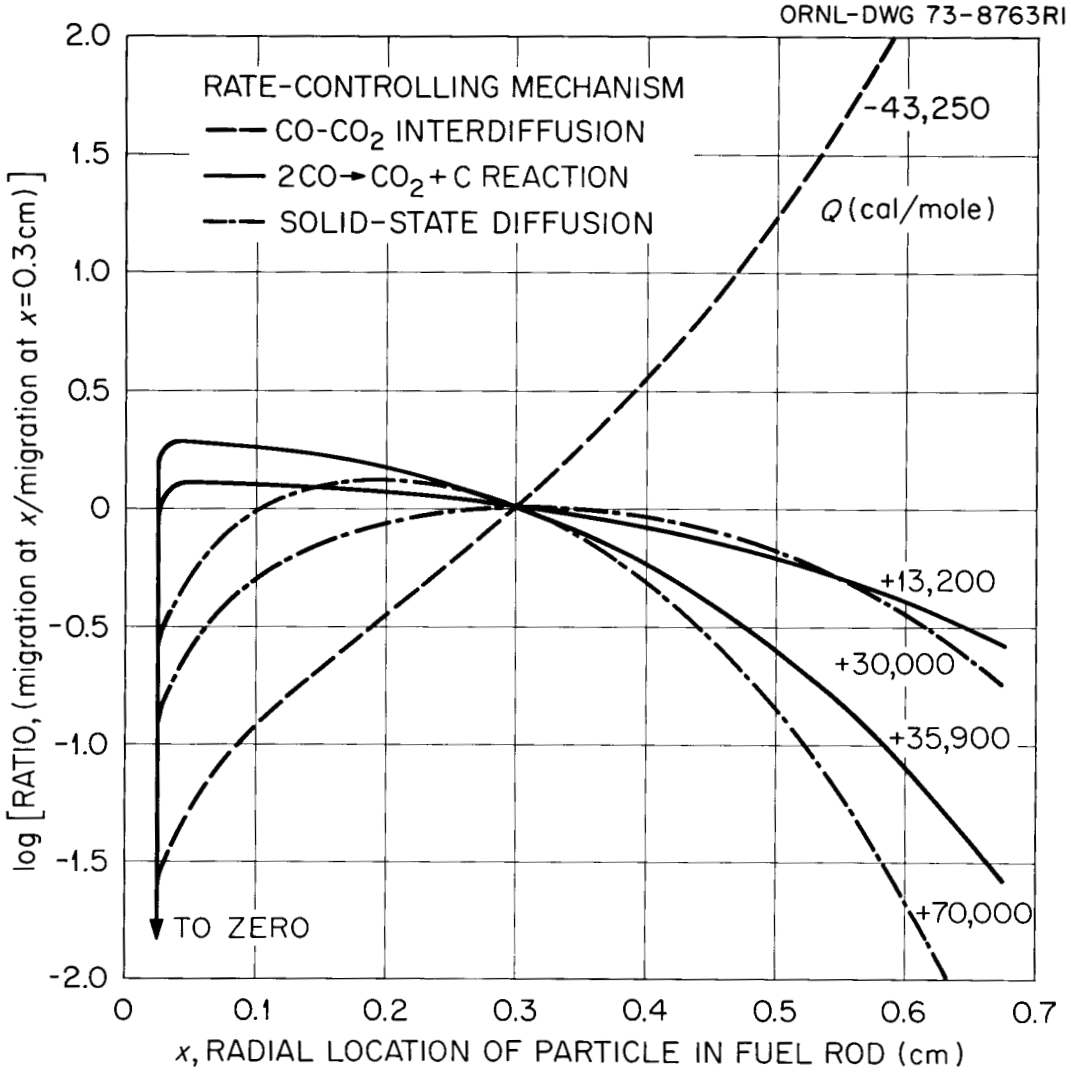

Fig. 18. Calculated Relative Kernel Migration Controlled by Indicated Mechanisms vs Radial Location of Particle Under Temperature Conditions Existing in Fuel Rod H-1-2.

Identification of the rate-controlling mechanism for kernel migration can tentatively be made. The choice is apparently between a solid-state diffusion mechanism and a reaction mechanism such as a gas-solid or solid-solid reaction. The calculated behavior in Fig. 18 indicates that reaction control should result in the largest migration near the center of the fuel rod. (This behavior assumes that the temperature-gradient-dependent mechanism that supplies reactants to the rate-controlling reaction proceeds at a rate sufficient to supply the reactants even as the temperature gradient approaches zero near the center of the fuel rod.) On the other hand, control by a solid-state diffusion mechanism results in a decrease in the kernel migration in particles near the center of the fuel rod. It appears that the observed behavior in rod H-1-2 follows this latter behavior, especially when one considers the kernels that did not migrate (Fig. 17). This indicates that a solid-state diffusion mechanism is controlling the kernel migration. Identification of solid-state diffusion as the rate-controlling mechanism for kernel migration in the other fuel rods that operated at much higher temperatures in the H-1 and H-2 experiments was not possible since some or all of the fuel particles had failed and converted to carbide within approximately the midradius of the fuel rod.[38]

A few cautionary statements about this analysis are in order at this point.

1. The analysis should be applied only to fuel rods for which all particles have coatings of sufficient integrity to retain the P_{CO} and the fission products. Such a requirement is necessary because these materials may strongly affect the general type and rate of the controlling mass-transport mechanism.

2. Identification of a controlling solid-state mechanism for kernel migration, such as was tentatively done for fuel rod H-1-2, does not necessarily identify the rate-controlling process for particle coating failure. This failure conceivably could be controlled by a faster mechanism such as $CO-CO_2$ diffusion.

3. It is well known that the rate-controlling mechanisms can be different at different temperatures (e.g., the case of grain-boundary vs lattice diffusion in solids). Thus the mechanism for mass transport in coated particles should be well established over the temperature range of interest before a quantitative first-principle correlation for that particular mechanism is used to interpret experimental data.

5. SUMMARY OF OXIDE FUEL BEHAVIOR

The thermodynamic behavior of unirradiated UO_2 and ThO_2 appears to be adequately defined, while some discrepancy exists in the data for PuO_{2-x}. The oxygen potential of the fuel oxide-fission product systems is essentially unexplored, but the few measurements of oxygen release (as carbon monoxide) during fission of $^{235}UO_2$ fall within the estimated range. These estimates also indicate that fission of $^{239}PuO_2$ releases substantially more oxygen than does $^{233}UO_2$ or $^{235}UO_2$ while the release for the latter two is approximately equivalent.

New methods have been developed to establish the rate-controlling mechanism for particle failure in oxide fuels. These methods result from the application of the theories for control of mass transport by either $CO-CO_2$ diffusion, the rate of decomposition of CO, or solid-state diffusion to the analysis of observed fuel migration under specific in-reactor

conditions of temperature and temperature gradient. Once the mechanism is identified, then quantitative expressions based on the theory for that particular mechanism can be derived for data correlation.

Application of the methods summarized above to the analysis of a recent irradiation of BISO-coated UO_2 particles indicated that the rate of kernel migration up the temperature gradient appeared to be controlled by a solid-state diffusion mechanism. Control of the kernel migration by CO-CO_2 diffusion was apparently not consistent with the experimental results. One possible technique to alleviate the rate of migration by the solid-state diffusion mechanism is the use of a higher-conductivity fuel rod matrix to lower the temperature gradient across the particle.

The possibility of the failure of the pyrolytic carbon coatings as the result of carbon removal by a CO-CO_2 diffusion mechanism, rather than by kernel migration, could not be excluded on the basis of the studies presented here. This is primarily because a reliable metallographic technique is not available for quantitatively measuring the pressure-vessel failure of the pyrolytic carbon coatings. It appears from the Dragon Project work that a more difficult and indirect technique, such as determining the time to the onset of in-reactor release of fission gas from the particles, might be used.

Theoretical calculations indicate that CO-CO_2 diffusion and the CO decomposition reaction should proceed at rates sufficiently rapid to cause early failure of the pyrolytic carbon coatings; however, such failure rates are not observed experimentally. Additional research needs to be performed to ascertain what processes may actually be operating in the fuel and fission product systems in order to propose techniques to significantly decrease the rates of these mechanisms.

Several other possible effects were not specifically considered here. These include effects of the neutron flux and fission fragment generation that might lead to rate differences between out-of-reactor and in-reactor experiments performed under identical conditions of temperature and temperature gradient. The effect of fission rate should be ascertained so that results obtained from accelerated tests in high-flux experimental reactors can be confidently applied to the design of long-life power reactor cores.

6. ACKNOWLEDGMENTS

The authors thank the several people who assisted with the preparation of this text. Dr. L. R. Shepherd, Chief Executive of the Dragon Project, kindly permitted us to include the results obtained by H. Bildstein and A. Strigl of OSGAE Seibersdorf. R. A. Olstad provided the temperature analysis of fuel rod H-1-2 and E. L. Long and N. A. Atchley assisted with the metallography. J. A. Lackey and A. P. Malinauskas provided a very valuable technical review of the text and M. G. Stewart, C. A. Proaps, M. M. Payne, and S. Peterson edited and typed the manuscript.

7. APPENDIX A: THERMODYNAMIC DATA FOR FUEL OXIDES AND CARBIDES

The free energy functions given in Table A-1 are used with other commonly available thermodynamic data to calculate the standard free energy change, $\Delta G°$, for a particular equilibrium reaction at a given temperature. Consider the hypothetical equilibrium

$$a\,A + b\,B \rightleftarrows c\,C + d\,D$$

and, for the sake of convenience, let "fef" represent $\frac{G°_T - H°_{298}}{T}$ and "H" represent $\Delta H°_{f_{298}}$, the heat of formation of a substance at 298°K. It can be shown that

$$\Delta G°_T = \left[c(fef)_C + d(fef)_D - a(fef)_A - b(fef)_B \right] T$$

$$+ cH_C + dH_D - aH_A - bH_B \quad .$$

The accuracy of the free energy functions for PuO_2 is dependent upon the accuracy of $S°_{298}$; this is as yet not well defined.[41]

Table A-1. Thermodynamic Data for Fuel Oxides and Carbides

Temperature (°K)	$-(G^\circ_T - H^\circ_{298})/T$ (cal mole^{-1} deg^{-1}) for:				
	UO_2 (ref. 42)	$UC_{1.93}$ (ref. 42)	ThO_2 (ref. 42)	ThC_2 (ref. 43)	PuO_2 (ref. 41)
298.15[a]	18.63	16.86	15.59	15.100	16.34
300.00	18.63	16.86	15.59	15.100	16.34
400.00	19.26	17.46	16.19	15.525	17.03
500.00	20.50	18.63	17.36	16.369	18.40
600.00	21.95	20.01	18.70	17.352	20.00
700.00	23.44	21.42	20.07	18.366	21.64
800.00	24.93	22.82	21.41	19.367	23.24
900.00	26.36	24.18	22.71	20.338	24.79
1000.00	27.74	25.48	23.95	21.271	26.27
1100.00	29.05	26.72	25.14	22.166	27.70
1200.00	30.29	27.91	26.27	23.021	29.05
1300.00	31.48	29.06	27.34	23.840	30.33
1400.00	32.60	30.16	28.38	24.625	31.54
1500.00	33.68	31.22	29.36	25.378	32.71
1600.00	34.70	32.25	30.31	26.102	33.81
1700.00	35.68	33.26	31.22	26.798	34.88
1800.00	36.62	34.24	32.09	27.468	35.89
1900.00	37.53	35.20	32.93	28.116	-
2000.00	38.40	36.14	33.74	28.741	-
2100.00	39.25	37.10	34.53	29.346	
2200.00	40.08	38.06	35.29	29.933	
2300.00	40.89	38.99	36.02	30.502	
2400.00	41.68	39.90	36.74	31.055	
2500.00	42.46	40.79	37.43	31.592	
2600.00	43.23	41.66	38.10	32.115	
2700.00	43.99	42.51	38.76	32.625	
2800.00	44.74	43.35	39.40	33.122	
2900.00	45.48	44.17	40.02	33.607	
3000.00	46.23	44.98	40.63		
	$\Delta H^\circ_{f_{298}}$ (kcal/mole)				
	-259.2 (ref. 43)	-20.8 (ref. 44)	-293.2 (ref. 45)	-46.6 (ref. 43)	-252 (ref. 46)

[a]At T = 298, $(G^\circ_{298} - H^\circ_{298})/T \equiv S^\circ_{298}$.

8. APPENDIX B: DERIVATION OF EQUATIONS FOR TRANSPORT OF CARBON BY $CO-CO_2$ DIFFUSION

The mathematical model to be developed here for carbon transport via $CO-CO_2$ diffusion is based primarily on the general equations developed by Schafer[47] for chemical transport reactions occurring in a temperature gradient. Spear[48] has also published a useful review of the regulating principles and application of these reactions. Consider the general reaction

$$iA_{(s)} + \ell B_{(g)} = jE_{(g)} \quad . \tag{B1}$$

The number of moles of solid material transported, n_A, as a result of gas-phase transport is obtained from the stoichiometry of the reaction and is

$$n_A = \frac{i}{\ell} n_B = \frac{i}{j} n_E \quad . \tag{B2}$$

In terms of the fluxes in the system, Eq. (B2) becomes

$$J_A = -\frac{i}{\ell} J_B = \frac{i}{j} J_E \quad , \tag{B3}$$

in which J_A, J_B, and J_E are the fluxes of material transported in moles cm^{-2} sec^{-1}. If reaction (B1) results in a net change in the number of moles of gas ($i \neq j$), then Schafer[47] develops his treatment under the constraint of constant total pressure at all points within the system. Consequently, the transport of gases B and E occurs by diffusion resulting from the equal and opposite concentration gradients of B and E and from the flow of the entire gaseous mass from the area where the chemical

reaction would otherwise produce a net increase in the number of moles of gas.

Schafer's[47] equations were expressed in terms of concentrations, C_i, rather than in terms of the partial pressures used here. Since $C_i = P_i/R_1T$, then

$$\frac{dC_i}{dT} = \frac{1}{R_1T}\left(\frac{dP_i}{dT} - \frac{P_i}{T}\right) , \tag{B4}$$

in which R_1 = 82.05 atm-cm^2-mole^{-1}-°K^{-1}. The term P_i/T can be shown to be insignificant for the C-CO-CO_2 system. For this system,

$$C(s) + CO_2(g) \rightarrow 2CO(g) , \tag{B5}$$

$$P = P_{CO} + P_{CO_2} . \tag{B6}$$

Since in Schafer's [47] analysis P is everywhere constant, dP/dT = 0, and then

$$dP_{CO}/dT = -dP_{CO_2}/dT . \tag{B7}$$

Also, one obtains

$$J_{CO} = -\frac{D}{R_1T}\frac{dP_{CO}}{dT}\frac{dT}{dx} + \frac{P_{CO}}{R_1T}w , \tag{B8}$$

$$J_{CO_2} = -\frac{D}{R_1T}\frac{dP_{CO_2}}{dT}\frac{dT}{dx} + \frac{P_{CO_2}}{R_1T}w , \tag{B9}$$

in which previously undefined terms are:

w = velocity of the total gaseous mass, cm/sec,

x = distance, cm.

In addition, the quantity D is defined by Schafer[47] as the diffusion coefficient (in cm^2/sec) for, in this case, the $CO-CO_2$ gas mixture under the experimental conditions of temperature and pressure; we will define this more rigorously in the next paragraph. Schafer et al.[49] manipulate Eqs. (B8) and (B9) under the constraints of Eqs. (B6) and (B7) to eliminate w, with the general result that

$$J_{CO} = -\frac{D}{R_1 T}\left(\frac{dP_{CO}}{dT}\frac{dT}{dx}\right)\frac{j(P_{CO} + P_{CO_2})}{jP_{CO_2} + \ell P_{CO}} \tag{B10}$$

$$J_{CO_2} = -\frac{D}{RT}\left(\frac{dP_{CO_2}}{dT}\frac{dT}{dx}\right)\frac{\ell(P_{CO} + P_{CO_2})}{jP_{CO_2} + \ell P_{CO}} \quad . \tag{B11}$$

For the $C-CO-CO_2$ reaction, $j = 2$ and $\ell = 1$.

The work of Malinauskas et al.[50] and a few simplifications of Eq. (B11) permit a more definitive evaluation of the term D used by Schafer.[47] If one starts with Eq. (41) of ref. 50 and derives an expression for J_{CO_2} under the conditions defined by Schafer et al.,[49] one obtains

$$J_{CO_2} = -\frac{\ell}{R_1 T}\frac{dP_{CO_2}}{dT}\frac{dT}{dx}\frac{D_1 D_2}{\ell D_2 + X_1(jD_1 - \ell D_2)} \quad , \tag{B12}$$

in which

$$1 = CO_2,$$

$$2 = CO,$$

$$D_1 = \frac{D_{12}\, D_{1K}}{D_{12} + D_{1K}} \, ,$$

$$D_2 = \frac{D_{12}\, D_{2K}}{D_{12} + D_{2K}} \, ,$$

and

$D_{12} = D_{21}$ = interdiffusion coefficient for a $CO-CO_2$ gas mixture space, cm^2/sec,

D_{1K}, D_{2K} = Knudsen diffusion coefficients, cm^2/sec,

X_1 = mole fraction CO_2 in the $CO-CO_2$ mixture.

Since $X_1 << 1$ for the usual conditions in coated particles, Eq. (B12) can be simplified, with little error, to

$$J_{CO_2} = -\frac{D_1}{RT}\frac{dP_{CO_2}}{dT}\frac{dT}{dx} \quad . \tag{B13}$$

Schafer[47] uses a similar simplification of Eq. (B11) for the condition equivalent to $X_1 << 1$, namely,

$$J_{CO_2} = -\frac{D}{RT}\frac{dP_{CO_2}}{dT}\frac{dT}{dx} \quad . \tag{B14}$$

A comparison of the latter two equations reveals that, to a first approximation, $D = D_1$. For gas pressures in the range of those found in coated particles, $D_1 = D_{12}$.[51] Having established this relationship, the treatment of the more rigorously derived Eqs. (B10) and (B11) is resumed.

The thermodynamic definition of P_{CO} and P_{CO_2} can be incorporated into Eq. (B9). At equilibrium, P_{CO_2} is given by

$$P_{CO_2} = P_{CO}^{\ 2}/K \quad , \tag{B15}$$

in which K is the equilibrium constant for reaction (B5). The term dP_{CO_2}/dT is obtained by differentiating Eq. (B15) with respect to temperature at constant total pressure, whence

$$\frac{dK}{dT} = \frac{\Delta H^\circ K}{RT^2} \tag{B16}$$

and

$$\frac{dP_{CO_2}}{dT} \cong - \frac{P_{CO}^2 \Delta H^\circ}{RT^2 K\ (1 + 2P_{CO_2}/P_{CO})} , \tag{B17}$$

in which

R = gas constant, 1.987 cal mole^{-1} °K^{-1},

ΔH° = standard enthalpy of reaction (B5) at temperature, cal/mole.

With the use of Eq. (B3) to give $J_C = -J_{CO_2}$, one thus obtains

$$J_C = - \frac{PD_{12}}{RR_1T^3} \frac{dT}{dx} \frac{P_{CO}\Delta H^\circ}{K(1 + 2P_{CO_2}/P_{CO})^2} . \tag{B18}$$

Another driving force considered for carbon transport was thermal diffusion in a CO-CO_2 gas mixture. For this purpose one compares the driving force dX_1/dT with k_t/T,[52] where k_t is the separation factor for thermal diffusion under steady-state conditions and X_1 is the mole fraction of carbon dioxide. An expression for k_t can be obtained from the work of Ibbs and Underwood,[53] who investigated thermal diffusion in CO-CO_2 mixtures at ~ 350°K; the results of their work lead to the approximate relation

$$k_t = 0.01\ X_1 \text{ for } 0 \leq X_1 \leq 0.4.$$

Therefore, it can be shown that the ratio of the driving forces is

$$\frac{dX_1}{dT}/(k_t/T) = \frac{\Delta H^\circ}{RT(1 + 2P_{CO_2}/P_{CO})} \left(\frac{1}{0.01}\right) . \tag{B19}$$

Since $\Delta H° \approx 40{,}000$ cal/mole for $1000 \leq T \leq 2500°K$, the value of the ratio is about 500, even under the most conservative conditions of $P_{CO_2}/P_{CO} = 1.0$. Thus, thermal diffusion is not a significant driving force for the transport of carbon in a coated particle.

The application of Eq. (B18) to the analysis of experimental data is facilitated by calculating a rate constant that contains several of the terms in Eq. (B18) and is defined as follows:

$$k = \frac{(P_{CO} + P_{CO_2})D_{12} \quad (53{,}300 \times 3600)\ \Delta H°}{RR_1T^3\ K(1 + 2P_{CO_2}/P_{CO})^2} \quad . \qquad \text{(B20)}$$

Thence Eq. (B18) can be expressed as

$$J_C' = -k\ P_{CO}\ \frac{dT}{dx} \quad , \qquad \text{(B21)}$$

in which J_C' = μm of carbon per hour.

Mason and Marrero[54] give

$$(P_{CO} + P_{CO_2})D_{12} = 5.77 \times 10^{-6}\ T^{1.803}\ \text{atm-cm}^2/\text{sec} \qquad \text{(B22)}$$

for the temperature range of interest here; this product is pressure independent and, within a few percent, independent of composition in the CO-CO_2 system.[54] The product of the constants 53,300 μm-cm^2 carbon/mole and 3600 sec/hr converts the units for the flux of carbon in moles of CO_2/cm^2-sec to the practically useful units of micrometers of carbon per hour. The rate constant was evaluated at $0.01 \leq P \leq 10^4$ atm as a function of temperature from thermodynamic data[10] for $\Delta H°$ and K for both carbon monoxide and carbon dioxide; the results are given in Fig. B-1. The

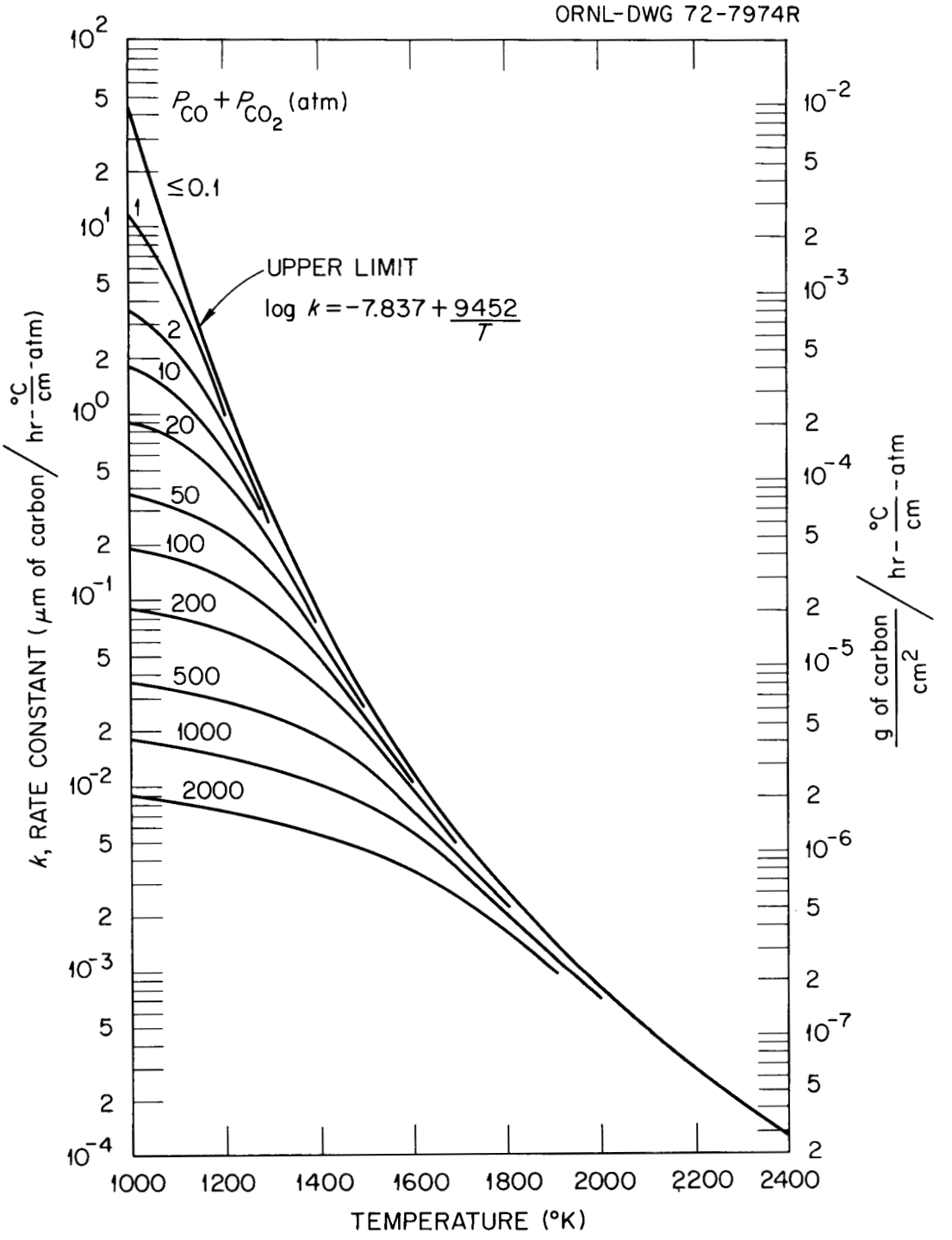

Fig. B-1. Temperature and Pressure Dependence of the Rate Constant, k, for $CO-CO_2$ Interdiffusion in a Temperature Gradient.

upper limit of k in Fig. B-1 is designated as k_ℓ and can be represented within 1.5% by

$$\log k_\ell = -7.837 + 9452/T \quad . \tag{B23}$$

The values of k below this upper limit merely reflect the effect of the term $(1 + 2P_{CO_2}/P_{CO})^2$ in Eq. (B20) becoming greater than unity. Here the term $2P_{CO_2}/P_{CO}$ becomes significant at lower temperatures and also as $P_{CO} + P_{CO_2}$ increases to large values, as can be seen qualitatively in Fig. 1.

There are two additional modifications to be made to Eq. (B21) before it may be applied to a coated-particle system. These occur because the diffusion takes place in a porous buffer layer and in the presence of coating gases, krypton and xenon. For diffusion of gases in porous media such as the pyrocarbon buffer layer, the observed value of the diffusion coefficient is $\frac{\varepsilon'}{q'} D_{12}$, where $\frac{\varepsilon'}{q'}$ is the ratio of the observed diffusion coefficient to that in free space and is less than unity.[47] This effect is incorporated into Eq. (B21) to give:

$$J_C' = -\frac{\varepsilon'}{q'} k P_{CO} \frac{dT}{dx} \quad . \tag{B24}$$

There are two effects of the additional gases on the carbon transport calculated for the CO-CO_2 system; both effects are reflected in the term PD_{12}. Now the term becomes $(\varepsilon P_i)D_{123\ldots n}$, in which the total pressure is the sum of the partial pressures of all gaseous species present in the system and $D_{123\ldots n}$ is the diffusion coefficient of carbon dioxide in the n-component gas mixture. However, the latter effect results in

a diffusion constant that is about 0.75 of that calculated for the $CO-CO_2$ system. This effect was not considered to be important to these calculations; however, the additional gases from the coating process and, primarily, from fission affect the rate of carbon transport by an order of magnitude or more.

The effect of these additional gases on the carbon transport calculated for the $CO-CO_2$ system is accommodated in the following manner. Consider the ratio, r, that is defined as

$$r = \frac{\text{flux of carbon in a system consisting of CO, } CO_2\text{, and other gases}}{\text{flux of carbon in a system consisting of CO and } CO_2 \text{ only}}$$

$$= \frac{P_{CO} + P_{CO_2}}{P_{CO} + P_{CO_2} + P_g + nRTF/a\theta} , \qquad \text{(B25)}$$

in which

P_g = pressure of residual gases from the coating operation, atm;

n = moles of gaseous fission products (excluding carbon monoxide) per mole of oxide per % FIMA;

F = % FIMA;

a = ratio, void space in the fuel kernel and the porous pyrocarbon layer to the superficial kernel volume;

θ = molar volume of the oxide kernel, e.g., 24.6 cm^3/mole for UO_2

$nRTF/a\theta$ = pressure of gaseous fission products, atm.

The effect of the additional gases on the flux of carbon, Eq. (B24), is thus accommodated by multiplying Eq. (B24) by r.

There are three final expressions for the calculation of the gas-phase

transport of carbon, each resulting from a particular mathematical treatment of different particle heat treatment and irradiation conditions. First, for out-of-reactor experiments with either as-coated or irradiated particles, the equation for carbon transport is:

$$y = \frac{\varepsilon'}{q'} k \frac{dT}{dx} P_{CO} \, r \, t \, , \tag{26}$$

in which

y = μm of carbon transported

t = time, hr.

Here the value of k is chosen from Fig. B-1 for the $P_{CO} + P_{CO_2}$ that exists in the particle at a given temperature. The second equation is developed for in-reactor tests. Under irradiation conditions, the ratio, r, changes because the pressure of fission gases, P_{CO}, and P_{CO_2} increases with burnup. The average value of the ratio, $\bar{r}$, between any initial and final state (burnup) can be determined via the mean-value theorem. For this case, the transport of carbon is described by the equation

$$y = \frac{\varepsilon'}{q'} k_\ell \frac{dT}{dx} \frac{(t_f - t_i)}{(F_f - F_i)} \int_{F_i}^{F_f} \frac{P_{CO} \, S_1}{(1 + 2P_{CO_2}/P_{CO})^2 \, S_2} \, dF \quad . \tag{B27}$$

The integral in Eq. (B27) would normally be evaluated with a computer by using Simpson's rule. A third equation can be derived from Eq. (B27) for the special case that P_{CO} and P_{CO_2} are chemically buffered, that is invariant with fission. If n, a, and θ are also assumed invariant and F_i and $t_i = 0$, one obtains

$$y_f = \frac{t_f \frac{dT}{dx} \frac{\varepsilon'}{q'} k \, (P_{CO} + P_{CO_2}) P_{CO}}{F_f (nRT/a\theta)} \ln \left[1 + \frac{(nRT/a\theta) F_f}{P_{CO} + P_{CO_2} + P_g} \right], \qquad \text{(B28)}$$

in which k is obtained from Fig. B-1 for the particular temperature and for the value of $P_{CO} + P_{CO_2}$ established by the buffering equilibrium.

9. DEFINITION OF SYMBOLS

a	Ratio, void space in the fuel kernel and the porous pyrocarbon layer/superficial kernel volume
a_o	Center-line temperature in a fuel rod, °K
a_2	$q/4\pi K_{Th} r_r^2$, Eq. (22), °C/cm^2
α	Temperature ratio, Eq. (18)
α'	Ratio of value of integrals, Eq. (19)
α_1	Proportionality constant, Eqs. (12a) and (12b), (μm/hr) °K^{-1} (°C/cm)$^{-1}$ (% FIMA/hr)$^{-1}$
α_2	Proportionality constant, Eqs. (14a) and (14b), (μm/hr) °K^{-1} hr^{-1} (% FIMA/hr)$^{-1}$
α_3	Proportionality constant, Eqs. (15a) and (15b), μm/hr
α_4	Proportionality constant or kernel migration coefficient, Eqs. (16a) and (16b), (cm/sec) °K^2 (°C/cm)$^{-1}$
α_5	Proportionality constant, Eqs. (17a) and (17b), (cm/sec) °K (°C/cm)$^{-1}$
C	Concentration, moles/cm^3
D	(Schafer's definition) diffusion coefficient for the gas mixture under experimental conditions of pressure and temperature, cm^2/sec
D_{12}	CO-CO_2 interdiffusion coefficient, cm/sec
$\Delta H°$	Standard enthalpy of reaction (B5), cal/mole
$\Delta H_1°$	Standard enthalpy of reaction (8), cal/mole
ΔP_{CO}	Pressure differential of carbon monoxide, atm
ε'/q'	Ratio, observed diffusion coefficient to that in free space, dimensionless

f	Final
F	% FIMA (Fissions per Initial Heavy Metal Atom)
$\bar{h}_j$	Heat of solution (partial molar enthalpy) of species j, cal/mole
i	Initial; number of moles
j	Number of moles; species
J	General symbol for gas flux, moles cm^{-2} sec^{-1}
k_t	Separation factor for thermal diffusion, dimensionless
k	Rate constant for $CO-CO_2$ diffusion, Fig. B-1, μm of carbon hr^{-1} $(°C/cm)^{-1}$ $(atm)^{-1}$
K	Equilibrium constant for reaction (B5), atm
K_{th}	Thermal conductivity, w cm^{-1} $°C^{-1}$
k_ℓ	Upper limit of rate constant for $CO-CO_2$ diffusion, Fig. B-1, Eq. (B23), μm of carbon hr^{-1} $(°C/hr)^{-1}$ atm^{-1}
ℓ	Number of moles
ℓ_B	Thickness of carbon buffer layer in a coated particle, μm
m	Moles of oxygen (as O) released from an oxide kernel per mole of oxide per % FIMA; $m = m_{CO} + 2m_{CO_2}$ in this report
m_{CO}, m_{CO_2}	Moles of carbon monoxide or carbon dioxide produced as a result of oxygen release during fission per mole of fuel oxide per % FIMA
MO	Metal monoxide, used for fission products
$MO_{1.5}$	Metal sesquioxide, used for fission products
MO_2	Metal dioxide, used for fission products
μm	Micrometers
μ	Chemical potential, cal/mole
n	Moles of gaseous fission products (excluding carbon dioxide and carbon monoxide) per mole of oxide per % FIMA

n_A, n_B, n_E	Moles of species A, B, or E
O/M	Oxygen-to-metal ratio
P	$P_{CO} + P_{CO_2}$ (atm); total pressure in system (atm). Also used with a subscript to indicate partial pressures, atm
P_{fg}	Pressure of Xe + Kr, atm
P_g	Pressure of residual gases from the particle coating operation, atm
P_{CO}	Pressure of carbon monoxide, atm
q	Heat generation rate, W/cm
Q_j^*	Heat of transport of species j in an oxide kernel, cal/mole
Q	Activation energy, cal/mole
r_r	Radius of fuel rod, cm
r	Ratio, flux of carbon in a system consisting of CO, CO_2 and other gases to the flux of carbon in a system consisting of CO and CO_2 only
$\bar{r}$	Average of r during fission (mean-value theorem)
R_1	Gas constant, 82.05 atm-cm^2 mole^{-1} °K^{-1}
R	Gas constant, 1.987 cal mole^{-1} °K^{-1}
S_1	Sum, $P_{CO} + P_{CO_2}$, atm
S_2	Sum, $P_{CO} + P_{CO_2} + P_g + P_{fg}$, atm
S_3	$(1 + 2P_{CO_2}/P_{CO})^2$
S/V	Surface-to-volume ratio of a porous solid, cm^2/cm^3
t	Time, hr, sec
T	Temperature, °K
τ	Reciprocal temperature difference, °K^{-1}
Θ	Molar volume of fuel oxide, e.g., 24.6 cm^3/mole for UO_2

V_U	Valence of uranium
V_{Pu}	Valence of plutonium
V_{Th}	Valence of thorium, 4
w	Velocity of the total gaseous mass, cm/sec
x	Deviation from stoichiometry (dimensionless); distance parameter (cm)
X_1	Mole fraction of carbon dioxide in a $CO-CO_2$ mixture
y	Micrometers of carbon transported; movement of hot-side kernel-carbon interface, cm
Y	Ratio, moles of Pu to moles of (U + Pu)

10. REFERENCES

1. M. S. T. Price, J. R. G. Gough, and G. W. Horsley, "Fuel Element Fabrication for the Dragon Reactor Experiment," J. Brit. Nucl. Energy Soc. 5, 361-82 (1966).
2. H. W. Muller, C. B. van der Decken, U. Hennings, and W. Stummer, "The AVR Pebble Bed Reactor," Ibid. 5, 319-31 (1966).
3. R. C. Dahlberg, R. F. Turner, and W. V. Goedel, "Fort Saint Vrain - Core Design Characteristics," Nucl. Eng. Intrn. 14, 1073-77 (1969).
4. L. R. Shepherd, "Development of Coated Particle Fuels for High Temperature Reactors," J. Brit. Nucl. Energy Soc. 9, 173-88 (1970).
5. R. A. U. Huddle, "Fuel Elements for High Temperature Reactors: Basic Materials Philosophy of the Dragon Programme," Advanced and High-Temperature Gas-Cooled Reactors, Proc. Symp. Jülich, IAEA, Vienna, 631-45 (1968).
6. J. L. Kaae, D. W. Stevens, and C. S. Luby, "Prediction of the Irradiation Performance of Coated Particle Fuels by Stress-Analysis Models," Nucl. Technol. 10, 44-53 (1971).
7. J. W. Prados and T. G. Godfrey, STRETCH, A Computer Program for Predicting Coated-Particle Irradiation Behavior, Modification IV, ORNL-TM-2127 (April 1968).
8. H. Walther, Dragon Project, private communication.
9. R. H. Flowers and G. W. Horsley, The Influence of Oxide Kernels on the Manufacture and Performance of Coated Particle Fuel, Atomic Energy Research Establishment (England) Report AERE-R5949 (1968).

10. JANAF Thermochemical Tables, 2nd ed., NSRDS-NBS 37, D. R. Stull and H. Prophet, Project Directors, Supt. of Documents, Washington, D.C. (1971).

11. T. L. Markin, V. J. Wheeler, and R. J. Bones, "High Temperature Thermodynamic Data for $UO_{2\pm x}$," J. Inorg. Nucl. Chem. 30, 807-17 (1968).

12. E. A. Aitken, H. C. Brassfield, and R. E. Fryxell, "Thermodynamic Behavior of Hypostoichiometric UO_2," Thermodynamics, Vol. II, Proc. Symp. Vienna 1965, IAEA, Vienna, 435-53 (1966).

13. A. Pattoret, J. Drowart, and S. Smoes, "Etudes Thermodynamiques par Spectrometric de Masse sur le System Uranium-Oxygene," Thermodynamics of Nuclear Materials, 1967, Proc. Symp. Vienna, IAEA, Vienna, 613-36 (1968).

14. K. Hagemark and M. Broli, "Equilibrium Oxygen Pressures over the Non-stoichiometric Uranium Oxides UO_{2+x} and U_3O_{8-z} at Higher Temperatures," J. Inorg. Nucl. Chem. 28, 2837-50 (1966).

15. M. H. Rand and T. L. Markin, "Some Thermodynamic Aspects of $(U,Pu)O_2$ Solid Solutions and Their Use as Nuclear Fuels," Thermodynamics of Nuclear Fuels, 1967, Proc. Symp. Vienna, IAEA, Vienna, 637-50 (1968).

16. T. L. Markin and E. J. McIver, "Thermodynamic and Phase Studies for Plutonium and Uranium-Plutonium Oxides with Application to Compatibility Calculations," Plutonium 1965, Proc. Conf. London, 1965, Chapman and Hall, London, for Institute of Metals, 845-57 (1967).

17. R. E. Woodley, "Equilibrium Oxygen Potential-Composition Relations in $U_{0.75}Pu_{0.25}O_{2-x}$," J. Am. Ceram. Soc. 56, 116-19 (1973).

18. N. A. Javed and J. T. A. Roberts, Thermodynamic and Defect-Structure Studies in Mixed-Oxide Fuels, Argonne National Laboratory Report ANL-7901 (1972).

19. T. B. Lindemer and R. A. Bradley, "Kinetic Models for the Synthesis of $(U,Pu)O_{2-y}$ by Hydrogen-Reduction and Carbothermic Techniques," J. Nucl. Mater. 41, 293-302 (1971).

20. R. Benz, "Thorium—Thorium Dioxide Phase Equilibria," J. Nucl. Mater. 29, 43-49 (1969).

21. R. J. Ackermann, E. G. Rauh, R. J. Thorn, and M. C. Cannon, "A Thermodynamic Study of the Thorium-Oxygen System at High Temperature," J. Phys. Chem. 67, 762-69 (1963).

22. S. Peterson and C. E. Curtis, Thorium Ceramics Data Manual, ORNL-4503, Vols. 1-5 (1970).

23. S. Aronson and J. C. Clayton, "Thermodynamic Properties of Nonstoichiometric Urania-Thoria Solid Solutions," J. Chem. Phys. 32, 749-54 (1960).

24. P. Kofstad, Nonstoichiometry, Diffusion, and Electrical Conductivity in Binary Metal Oxides, Wiley-Interscience, New York (1972).

25. M. J. Bell, ORIGEN—The ORNL Isotope Generation and Depletion Code, ORNL-4628 (1973).

26. L. W. Graham, "The Development and Performance of HTGR Core Materials," Gas-Cooled Reactor Information Meeting, Oak Ridge, Tennessee, CONF-700401 (April 1970), pp. 494-517.

27. H. Bildstein and A. Strigl, Determination of Gases in Low Enriched Coated Oxide Particles, O.E.C.D. High Temperature Reactor Project (England) D.P. Report 728 (1970). (Used by permission).

28. HTGR Base Program Quarterly Progress Report, Gulf General Atomic (USA) Report GA-A12515 (March 1973), pp. 79-89.

29. T. B. Lindemer and H. J. de Nordwall, "Analysis of Chemical Failure of Urania Fuel Particles in the HTGR," Am. Ceram. Soc. Bull. 54, 390 (1972).

30. T. B. Lindemer, "Fuel Migration Studies," pp. 112-13 in Gas-Cooled Reactor and Thorium Utilization Programs Ann. Progr. Rept. Sept. 30, 1971, ORNL-4760 (January 1973).

31. T. D. Gulden, "Carbon Thermal Diffusion in the UC_2-C System," J. Am. Ceram. Soc. 55, 14-18 (1972). [Also published as Gulf General Atomic (USA) Report GA-10520 (1971].

32. Public Service Co. of Colorado Quart. Progr. Rept., Gulf General Atomic Report Gulf-GA-10010 (Mar. 31, 1970), pp. 129-36.

33. C. B. Scott and O. M. Stansfield, Stability of Irradiated Coated-Particle Fuels in a Temperature Gradient, Gulf General Atomic Report Gulf-GA-A12081 (1972).

34. A. E. Reif, "A Study of the Reactions of Carbon Monoxide with Coke," J. Phys. Chem. 56, 778-84 (1952).

35. S. A. Pursley, R. A. Matula, and O. W. Witzell, "The Kinetics of Carbon Dioxide and Carbon Formation from Carbon Monoxide," J. Phys. Chem. 70, 3768-70 (1966).

36. W. J. Lackey, ORNL, private communication (May 1973).

37. E. A. Aitken, "Thermal Diffusion in Closed Oxide Fuel Systems," J. Nucl. Mater. 30, 62-73 (1969).

38. R. A. Olstad, A. R. Olsen, R. B. Fitts, E. R. Long, and T. B. Lindemer, An Irradiation of Candidate HTGR Fuels in the H-1 and H-2 Capsules, ORNL-TM-4397 (to be published).

39. H. S. Carslaw and J. C. Jaeger, Conduction of Heat in Solids, p. 191, Oxford University Press, London, 1959.

40. J. A. L. Robertson, $\int k d\Theta$ in Fuel Irradiations, Atomic Energy of Canada Report CRFD-835 (1959).

41. O. L. Kruger and H. Savage, "Heat Capacity and Thermodynamic Properties of Plutonium Dioxide," J. Chem. Phys. 49, 4540-44 (1968).

42. T. G. Godfrey, J. A. Wooley, and J. M. Leitnaker, Thermodynamic Functions of Nuclear Materials: UC, UC_2, UO_2, ThO_2, and UN, ORNL-TM-1596 (Rev.) (1966).

43. H. L. Schick, Thermodynamics of Certain Refractory Compounds, Vol. 2, p. 93, Academic, New York, 1966.

44. J. M. Leitnaker and T. G. Godfrey, "Thermodynamic Properties of Uranium Carbides via the U-C-O System," J. Chem. Eng. Data 11, 392-94 (1966).

45. E. L. Huber, Jr., C. E. Holley, Jr., and E. H. Meierkord, "Heat of Combustion of Thorium and Uranium Oxides," J. Am. Chem. Soc. 74, 3406-8 (1952).

46. G. L. Johnson, E. H. vanDeventer, O. L. Kruger, and W. N. Hubbard, "The Enthalpies of Formation of Plutonium Dioxide and Plutonium Mononitride," J. Chem. Thermo. 1, 89-98 (1969).

47. H. Schäfer, Chemical Transport Reactions, pp. 22-23, Academic, New York, 1964.

48. K. E. Spear, "Chemical Transport Reactions," J. Chem. Educ. 49, 81-86 (1972).

49. H. Schäfer, H. Jacob, and K. Etzel, "Über der Transport des Bodenkörpers in Temperaturgefälle mit Hilfe heterogener Gleichgewichte," Z. Anorg. Allgem. Chem. 286, 27-41 (1956).

50. A. P. Malinauskas, J. L. Rutherford, and R. B. Evans III, Gas Transport in MSRE Moderator Graphite. 1. Review of Theory and Counterdiffusion Experiments, ORNL-4148 (1967).

51. Ibid., p. 16.

52. S. W. Benson, The Foundation of Chemical Kinetics, p. 186, McGraw-Hill, New York, 1960.

53. T. L. Ibbs and L. Underwood, "A Comparison of the Behaviour in Thermal Diffusion of Nitrogen and Carbon Monoxide, and of Nitrous Oxide and Carbon Dioxide," Proc. Phys. Soc. 39, 227-37 (1927).

54. E. A. Mason and T. R. Marrero, "The Diffusion of Atoms and Molecules," p. 218 in Advances in Atomic and Molecular Physics, Vol. 6, Academic, New York, 1970.

ORNL-4926
UC-77 — Gas Cooled Reactor Technology

INTERNAL DISTRIBUTION

1. G. M. Adamson, Jr.
2. J. W. Anderson
3. H. F. Bauman
4. S. E. Beall
5. R. L. Beatty
6. M. Bender
7. L. L. Bennett
8. C. E. Bettis
9. R. E. Blanco
10. E. G. Bohlmann
11. E. S. Bomar
12. W. D. Bond
13. C. J. Borkowski
14. H. I. Bowers
15. R. A. Bradley
16. R. B. Briggs
17. R. E. Brooksbank
18. K. B. Brown
19. R. H. Bryan
20. O. W. Burke
21. J. P. Callahan
22. D. D. Cannon
23. A. J. Caputo
24. J. V. Cathcart
25. H. D. Cockran, Jr.
26. E. L. Compere
27. J. A. Conlin
28. J. H. Coobs
29. W. H. Cook
30. D. F. Cope/F. E. Dearing
31. D. A. Costanzo
32. W. B. Cottrell
33. J. A. Cox
34. F. L. Culler
35. J. E. Cunningham
36. F. C. Davis
37-57. H. J. de Nordwall
58. F. F. Dyer
59. W. P. Eatherly
60. R. B. Evans III
61. J. R. Engel
62. D. E. Ferguson
63. B. C. Finney
64. R. B. Fitts
65. C. L. Fitzgerald
66. A. P. Fraas
67. R. W. Glass
68. R. J. Gray
69. B. L. Greenstreet
70. W. R. Grimes
71. P. A. Haas
72. R. L. Hamner
73. W. O. Harms
74. F. E. Harrington
75. R. F. Hibbs
76. H. W. Hoffman
77. F. J. Homan
78. J. P. Jarvis
79. J. D. Jenkins
80-118. P. R. Kasten
119. R. J. Kedl
120. H. T. Kerr
121. W. J. Lackey
122. J. M. Leitnaker
123. C. E. Lamb
124. R. E. Leuze
125-145. T. B. Lindemer
146. E. L. Long, Jr.
147. A. W. Longest
148. A. L. Lotts
149. R. E. MacPherson
150. A. P. Malinauskas
151. W. J. Martin
152. W. R. Martin
153. H. C. McCurdy
154. W. T. McDuffee
155. D. L. McElroy
156. L. E. McNeese
157. A. B. Meservey
158. B. H. Montgomery
159. M. T. Morgan
160. F. H. Neill
161. J. P. Nichols
162. K. J. Notz
163. L. C. Oakes
164. R. A. Olstad
165. M. F. Osborne
166. P. Patriarca
167. W. H. Pechin
168. A. M. Perry
169. T. W. Pickel
170. J. M. Robbins

171. M. W. Rosenthal
172. P. Rubel
173. J. P. Sanders
174. C. D. Scott
175. J. L. Scott
176. J. D. Sease
177. J. H. Shaffer
178. G. M. Slaughter
179. J. W. Snider
180. R. S. Stone
181. K. R. Thoms
182. M. Tobias
183. D. B. Trauger
184. W. E. Unger
185. V. C. A. Vaughen
186. J. E. VanCleve
187. T. N. Washburn
188. D. C. Watkin
189. J. R. Weir
190. A. M. Weinberg
191. J. C. White
192. G. D. Whitman
193. R. G. Wymer
194-196. Central Research Library
197. ORNL — Y-12 Technical Library, Document Reference Section
198-220. Laboratory Records Department
221. Laboratory Records, ORNL R.C.
222. ORNL Patent Office
223. Patent Office, AEC, ORO
224. J. C. Frye (consultant)
225. C. H. Ice (consultant)
226. J. J. Katz (consultant)
227. E. A. Mason (consultant)
228. Peter Murray (consultant)
229. R. B. Richards (consultant)

EXTERNAL DISTRIBUTION

230. Director, USAEC Division of Reactor Research and Development, Washington, D.C. 20545
231. USAEC-RRD Senior Site Representative, Oak Ridge National Laboratory, P. O. Box X, Oak Ridge, TN 37830
232. Research and Technical Support Division, USAEC Oak Ridge Operations Office, P. O. Box E, Oak Ridge, TN 37830
233-377. For distribution as shown in TID-4500 Distribution Category, UC-77, Gas Cooled Reactor Technology

☆U.S. GOVERNMENT PRINTING OFFICE: 1973-747-302/99